PB-229 798

REMOTE SENSING OF POLLUTANTS IN GAS PLUMES BY INFRARED EMISSION RADIOMETRY-SPECTROSCOPY

H. William Prengle, Jr., et al

Houston University

Prepared for:

Public Health Service

1 March 1972

DISTRIBUTED BY:

NTIS

National Technical Information Service
U. S. DEPARTMENT OF COMMERCE
5285 Port Royal Road, Springfield Va. 22151

PB 229 798

Remote Sensing of Pollutants in Gas Plumes by Infrared Emission Radiometry-Spectroscopy

by

H. William Prengle, Jr.
Professor of Chemical Engineering
Principal Investigator

Air Pollution Research Grant AP 00578

March 1, 1972

University of Houston
Chemical Engineering Department
Houston, Texas (77004)

NATIONAL TECHNICAL INFORMATION SERVICE

UNIVERSITY OF HOUSTON
CHEMICAL ENGINEERING DEPARTMENT

FINAL REPORT: Air Pollution Research Grant AP 00578

REMOTE SENSING OF POLLUTANTS IN GAS PLUMES BY INFRARED EMISSION RADIOMETRY-SPECTROSCOPY

by

H. William Prengle, Jr. D.Sc.
Professor of Chemical Engineering
Principal Investigator

and

C. A. Morgan, Ph.D.
C. S. Fang, Ph.D.
P. Campani, M.S.
W. W. Wu, M.S.
L. K. Huang, M.S.
E. G. Felton, M.S.
U. Mahagaokar, B.S.

∘ IRES PROJECT ∘

March 1, 1972

[RESTRICTED ∘ Not for general release until Sept. 1, 1972 because of publication commitments]

Reproduced by
NATIONAL TECHNICAL
INFORMATION SERVICE
U S Department of Commerce
Springfield VA 22151

•TABLE OF CONTENTS•

		page
I.	PROJECT SUMMARY	1
II.	INFRARED REMOTE SENSING OF POLLUTANTS IN GAS PLUMES	3
	Abstract	3
	Introduction	4
	The Equipment System	7
	Radiant Signals From a Gas Plume	12
	Temperature Measurement -- Total Energy Method	16
	Pollutant Concentration Measurement	18
	Laboratory and Field Tests	23
	Results and Correlations	25
	Conclusions	34
	Nomenclature	37
	Acknowledgment	39
	Literature Cited	39
	Figures: 1 - Equipment System	8
	2 - Assembled Equipment System	9
	3 - Black Body Function	14
	4 - Pollutant Identification Frequencies	21
	5 - Plume Field-Of-View	24
	6 - Generalized Temperature Function	29
	7 - Turbulent Temperature Fluctuations	30
	8 - Generalized Pollutant Function	32
	Tables: I.- Selected Infrared Bands	20
	II.- Constants For Adsorption Coefficient Functions	22
	III.- Fuel & Stack Gas Analysis	26

		page
	IV.- System Parameters	28
	V.- Typical Run Data	33
III.	INFRARED ABSORPTION COEFFICIENTS FOR CERTAIN POLLUTANT GASES	41
	Abstract	41
	Introduction	42
	Literature Search	44
	Experiments Conducted	49
	Experimental	50
	A. Apparatus	50
	B. Calculation of k_ν	51
	C. Error Analysis	52
	Results and Correlation	53
	Discussion	60
	Acknowledgment	61
	Literature Cited	63
	Figures: 1 - Carbon Dioxide at 15.0μ, T = 297.0°K	54
	2 - Carbon Dioxide at 4.26μ, T = 297.6°K	55
	3 - Temperature Effect, CO_2 at 15.0μ	56
	Tables: I.- Summary of Data from the Literature	45
	II.- Constants for Correlation Functions	57
	III.- Slopes cf. Square-Root Model	62
APPENDICES.		
	A. Temperature Runs	i
	B. Pollutant Concentration Runs	v

I. PROJECT SUMMARY

This report summarizes work started in the University of Houston Chemical Engineering Department in February 1968 on infrared emission spectroscopy (IRES Project) applied to the determination of pollutants in emerging hot gas plumes. Subsequently in June 1968 an HEW-PHS grant was received to study the possibility of remotely determining the "pollutants in chimney stack plumes". The grant covered a three year period plus a three month supplement until August 31, 1971.

The project was pursued along several lines of attack simultaneously:

1) Development of mathematical models for the transfer of spectral radiant energy from a remote hot gas envelop to a telescopic receiver system.

2) Selection and assembly of a telescopic-interferometer-spectrometer system, and operation of the system.

3) Laboratory measurement of infrared absorption coefficients for pollutant gas species.

4) Development of hybrid computational methods to process the output data to produce a final spectrogram of the source, and quantitatively determine the temperature and concentration of the pollutant species.

Briefly the radiometer spectrometer method consists of receiving infrared emission signals from a hot gas characteristic of each pollutant species; coadding many weak signals, and calculating by Fourier transform methods the spectra; then determining, a) the plume temperature, and b) the pollutant concentrations. Technically and operationally the method has the advantages of:

1) Remote sensing of pollutants from inaccessible emission sources and eliminating the necessity of taking gas samples.

2) Obtaining a composite strong signal (as a function of frequency) by coadding many weak signals.

3) Collecting information simultaneously on many chemical species which can be sorted out spectroscopically to premit their identification and concentration determination.

The initial objectives of the project have now been attained; conclusions from the work are as follows:

1) A remote sensing radiometer spectrometer system, based on interferometer Fourier spectroscopy, for quantitatively determining pollutants in hot gas plumes has been developed and demonstrated to be feasible.

2) Generalized temperature and concentration models, based on theory with the inclusion of certain empirical factors, have been developed and their applicability demonstrated.

3) The pollutants: CO, NO, unburned hydrocarbons, and combustion product olefins, have been quantatively determined. The range can be extended to include oxidation products (e.g. aldehydes) produced in the plume reactor as it emerges into the atmosphere.

4) Measurements at distances up to 100 m. and for plume temperatures < 400°K are presently within the state-of-the-art, and with improved equipment (more sensitive detectors, etc.) and refined procedures, the range could be substantially extended.

5) Temperatures can be determined at 65 m. distance to ± 10°K and concentrations to ± 28% of the measured value over the range 10 to 10^4 ppm.; it appears that the error limits can be reduced.

6) The system can be used to observe temperature and concentration gradients as a plume emerges from its source. Also turbulent fluctuating temperature values can be determined within 0 to 10°K about a mean value, on a 1 to 3 sec. interval, and it appears possible to observe fluctuating pollutant concentrations.

Work should be continued along lines indicated by the above conclusions.

The report which follows is presented in the form of two manuscripts which have been submitted for publication covering the work:

1) "Infrared Remote Sensing of Pollutants in Gas Plumes"; submitted to Environmental Science and Technology in January 1972 and is currently being reviewed for publication.

2) "Infrared Adsorption Coefficients for Certain Pollutant Gases"; has been accepted for publication by Applied Spectroscopy and will appear in the March-April 1972 issue.

II. INFRARED REMOTE SENSING OF POLLUTANTS IN GAS PLUMES

by

H.W. Prengle, Jr., C.A. Morgan, C.S. Fang*,
L.K. Huang, P. Campani, W.W. Wu

Chemical Engineering Department, University of Houston
Houston, Texas (77004)

ABSTRACT

Results of work on the application and development of quantitative methods for the determination of pollutants from emission sources by remote sensing, combining infrared radiometry and spectroscopy are presented and the method proved feasible. Generalized temperature and concentration models, based on the theory plus certain empirical factors have been developed and their applicability demonstrated.

Field measurements at 65 m. distance on gas fired power plant plumes at temperatures 500 - 600 °K were made and CO, NO and NO_2, CH_4 + saturates, and C_2H_4 + unsaturates, concentrations were determined. Temperatures can be determined to within ±10°K and concentrations to within ±28% of the value over the range 10 to 10^4ppm.

Extension of the method to temperature and concentration gradients and fluctuations in plumes due to chemical reactions, and measurements at greater distances appear to be feasible.

Index words: Remote sensing of pollutants; Infrared radiometry and emission spectroscopy of pollutants; Power plant pollutants.

December 1971

*Present address: Chemical Engineering Department, University of Southwestern Louisiana, Lafayette, La. (70501).

INTRODUCTION

A comprehensive atmospheric pollution monitoring system will require a number of techniques for the determination of the pollutants. Direct measurements on samples withdrawn from the atmosphere at periodic intervals is the method currently in use in the nation-wide CAMP system. At any given time, the level of atmospheric pollution involves the interaction of three factors (Hochheiser, Burmann, et al., 1971): ambient atmospheric concentrations, meteorological conditions, and emissions from polluting sources. Many of the latter are relatively inaccessible, e.g. plumes from tall stacks, and since it is highly desirable to measure pollutants at their source, they represent a special monitoring problem.

This paper presents the results of preliminary work on the application and development of quantitative methods for the determination of pollutants from emission sources by remote sensing, combining infrared radiometry and emission spectroscopy. As indicated by Rothschild (1971) in his Royal Society Lecture, the potentially harmful substances emitted into the atmosphere are,

CO, NO, unburned and pyrolyzed hydrocarbons. These are the ones of primary interest in this investigation, which when irradiated with sunlight and in the presence of oxygen react to produce additional harmful species.

Modern remote sensing techniques have been used in numerous applications, starting with infrared photography from aircraft and later from earth orbiting satellites. Several manned and unmanned satellites carried Michelson interferometers (Mertz, 1963; Block and Zachor, 1964; Lovett, Marcotte, et al., 1967) to obtain earth spectra, and more recently a Michelson interferometer was flown on Nimbus III (Hanel, Schlachman, et al., 1970; Wark, 1970) to obtain infrared emission spectra of the earth and its atmosphere. Planned for the next several years are the CARETS, ERTS, and SKYLAB projects (Anon., 1971), which will accomplish more extensive earth resource surveillance and obtain among other things, atmospheric pollution data.

The application of remote sensing techniques to the determination of pollutants from emission sources, and the application of interference spectroscopy has been discussed previously (Low,

1966; 1967; Low and Coleman, 1966). Also a number of papers have appeared on Fourier transform spectroscopy (Dunn and Block, 1969; Dunn and Foskett, 1971); two (Martin, 1966; Horlick, 1968) are particularly instructive. Remote signals from sources 10 to 100 m. distance at temperatures in the range of 500°K. are very weak; consequently, multiscan interference spectroscopy is ideally suited for this application.

In our configuration the basic optical element is the Michelson interferometer with one fixed and one movable mirror which scans the interference highs and lows at a known velocity and thereby obtains spectral information about the source in the form of an electrical signal from the detector called an interferogram. The interferogram frequencies depend on the frequency of the electromagnetic radiation received and the velocity of the mirror. Thus high frequency radiation is encoded into low frequency oscillations. Proper Fourier transformation of the complex wave function (interferogram) yields a spectrogram of the source, intensity vs. frequency.

THE EQUIPMENT SYSTEM.

As shown in Figure 1 the equipment system can be visualized as two parts: a) the signal receiving and data collecting sub-system, and b) the data processing sub-system.

The data collecting sub-system is a mobile unit, which can be conveniently transported by a small truck, and includes the following:

a)-a custom designed Cassegrain telescope, with 10" dia. x f/2 primary mirror, 2.8" dia. x f/2 secondary mirror; mounted on a Model 6312 Quick-Set Tripod, with Model 5692 dolly and Model 6222 gearhead with vernier tilt and pan;

b)-a Block Engineering Company Model 296 Interferometer Spectrometer, 2.8 to 15μ range, 0.50 cm^{-1} resolution, 0.10 cm^{-1} or better precision; and

c)-a Hewlett-Packard Model 3960 3 speed 4 channel Analog tape recorder.

The assembled equipment is shown in Figure 2.

The telescope provides a means of aiming the interferometer and collecting (magnifying) signals from various remote sources.

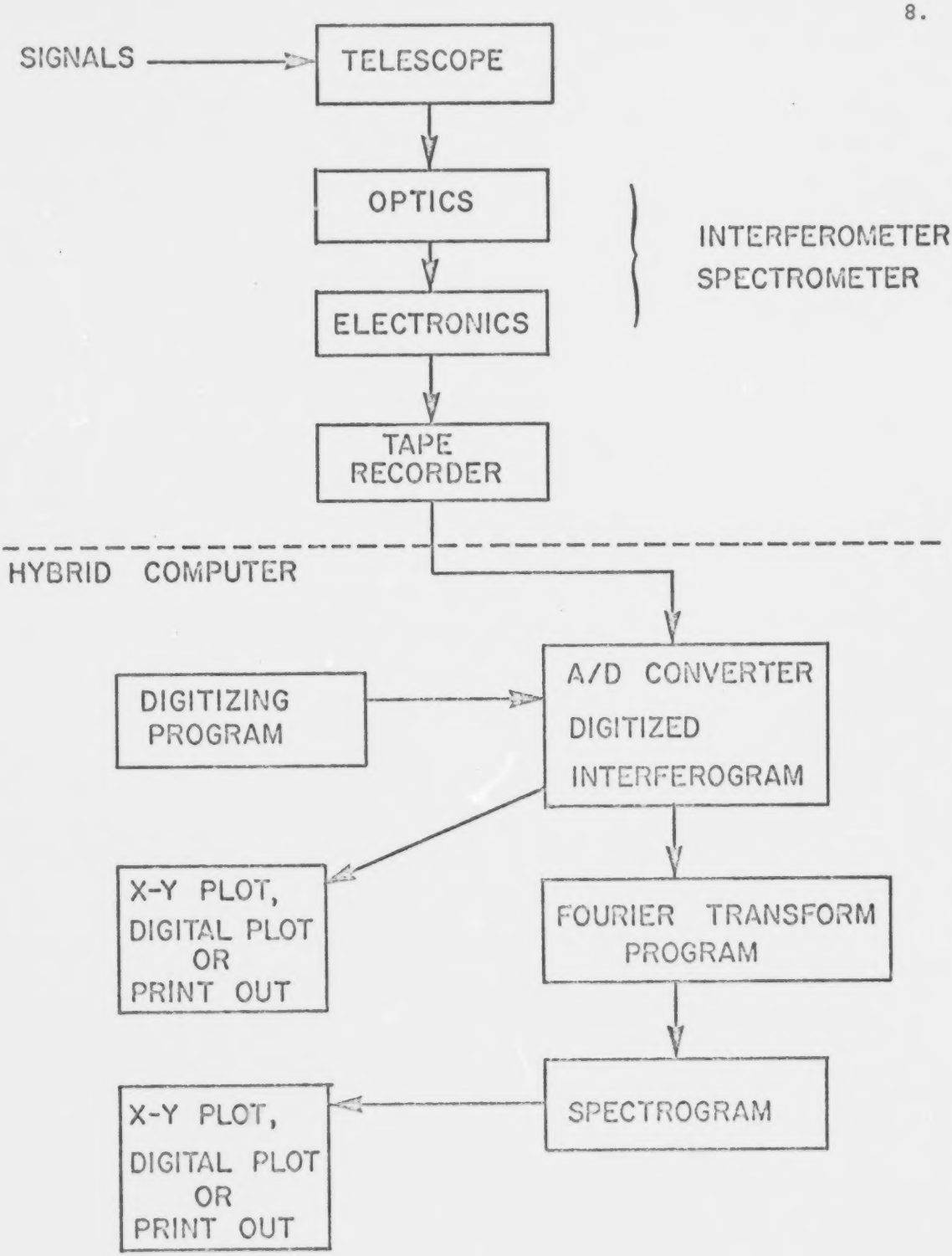

FIGURE I – EQUIPMENT SYSTEM

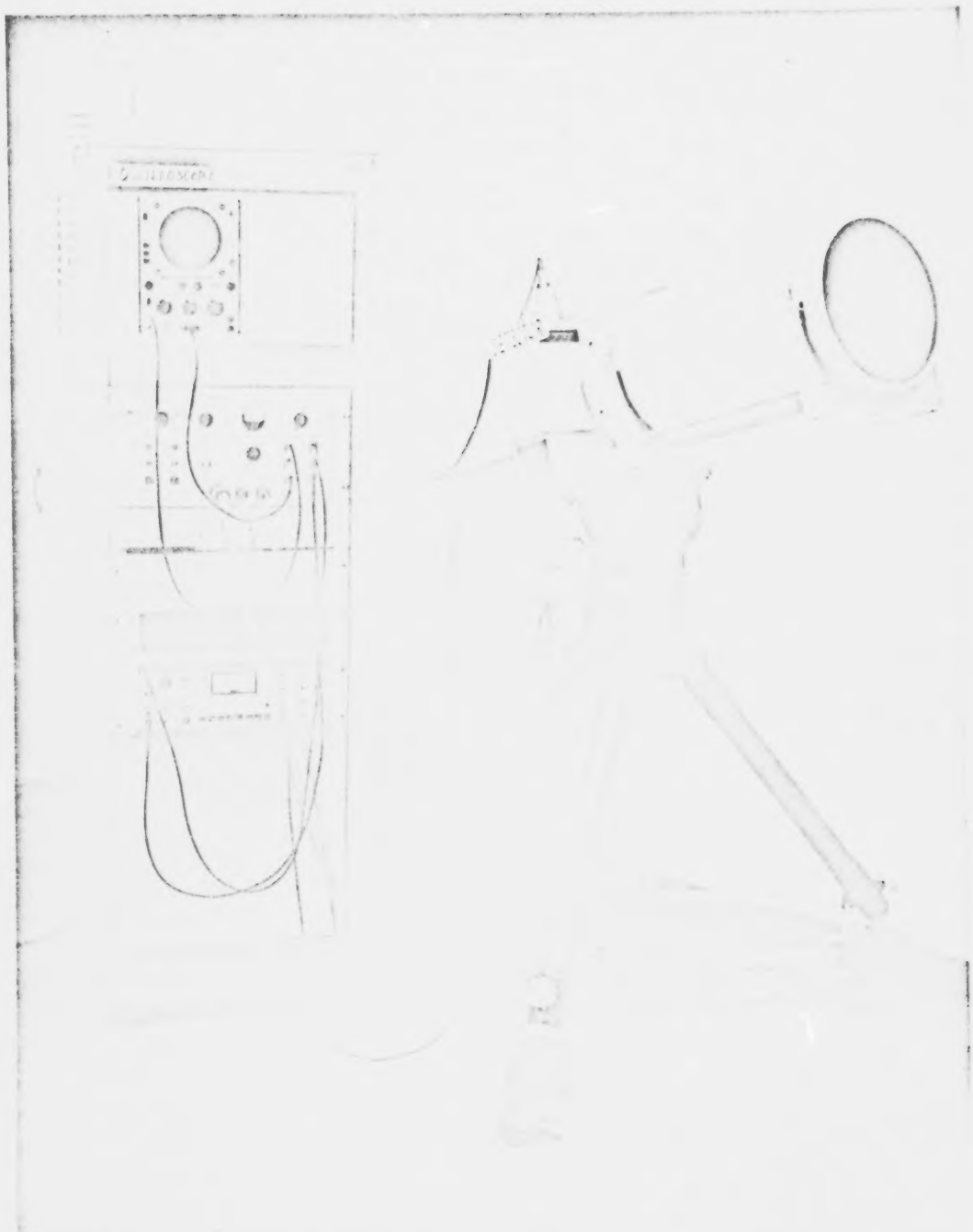

FIGURE 2 - ASSEMBLED EQUIPMENT SYSTEM

The optical head of the interferometer-spectrometer receives the energy emitted by the source and the Michelson interferometer scans the wave number range. The Optical retardation is accurately measured, within the precision of few angstroms, by a reference interferogram, generated by monochromatic light of a laser. The interferogram of the monochromatic light beam is generated by the movement of the same mirror which acts on the incoming energy beam. This interferogram, through a fringe counting device also gives with extreme precision the end point of the scanning range. The initial point of the scanning range is determined by a second reference interferogram of a white light beam, which ensures reproducibility of the initial point of each successive scanning range, and is the essential feature for the averaging of the signals.

The signals from the incoming energy beam and from the reference beams are collected by different detectors and transferred to the electronic part of the instrument, where they are amplified and given as output of the instrument.

The tape recorder is the last item of the chain of the data

collecting system. It is of instrumentation quality, has four channels, and records the output of the interferometer. The taped signals consist of an interferogram, trigger, and clock. The interferogram is a composite of sine waves of different amplitudes and frequencies from 300 to 3000 Hz. The trigger is a square wave pulse derived from the white light reference interferogram which occurs once at the beginning of every scan of the interferometer. The time per scan is related to the length of scan which determines the spectral resolution and which is selectable by means of front-panel control from 0.5 to 4.0 wavenumbers. The clock signal is a square wave train derived from the monochromatic reference interferogram required to command the analog-to-digital conversion process, and the frequency of the clock is selected from the front panel in multiples of a laser reference frequency. The trigger and clock are combined into one interferometer signal output called "synch" and is used to command the analog-to-digital converters to start converting on receipt of clock pulses. Signal and "synch" outputs are tape recorded and stored until required for digitization and further data reduction, as indicated in Figure 1.

The data processing sub-system is a Hybrid Systems SS-100/IBM

360 Hybrid Computer, and processes the taped data in the following steps:

a.- digitizes the recorded data in the A/D converter.

b.- averages the various scans to increase the signal/noise ratio and subtracts the d.c. offset voltage obtaining a digital interferogram.

c.- accomplishes a Fourier transformation of the digital interferogram (Block Engineering, 1967), using the well known fast Fourier transform algorithm (Cooley and Tukey, 1965) to obtain the spectrogram (intensity vs. wavenumber) of the source.

The interferogram and spectrogram are used in a manner described later to obtain the temperature and composition of the source.

RADIANT SIGNALS FROM A GAS PLUME.

A number of mathematical models for the remote sensing of infrared radiation from molecular species in a hot gas plume were examined: 3-dimensional spherical and cylindrical, and 2-dimensional geometry. When the distance is great compared to the plume and receiver sizes, a generalized model can be used to

good approximation.

For a very narrow band $\Delta\tilde{\nu}(cm^{-1})$, produced by a particular molecular species at $\tilde{\nu}$, the radiant flux can be written as*,

$$J = A_m X^2 \int_{\Delta\tilde{\nu}} \tau_a \, W_{B\tilde{\nu}} \, \varepsilon_{\tilde{\nu}} d\tilde{\nu} \qquad (1)$$

(millewatts)

and the irradiance of the receiver (telescope mirror) is,

$$H \equiv \left(\frac{J}{A_m}\right) = \tau_a \, X^2 \, \bar{W}_{B\Delta\tilde{\nu}} \, \varepsilon_{\tilde{\nu}} \Delta\tilde{\nu} \qquad (2)$$

(millewatts/cm^2)

where the blackbody function is given by,

$$W_{B\tilde{\nu}}(T) = \frac{2\pi k c^2 \tilde{\nu}^3}{\left(e^{\frac{hc\tilde{\nu}}{kT}} - 1\right)} = \frac{c_1 \tilde{\nu}^3}{\left(e^{\frac{c_2 \tilde{\nu}}{T}} - 1\right)} \qquad (3)$$

(millewatts/cm^2/cm^{-1})

and shown in Figure 3 for the range of temperatures involved.

The Cassegrain telescope transmits the radiation into the Michaelson interferometer where the beam splitter divides the radiation, 50-50% transmitted and reflected. When the optical path lengths of the reflected and transmitted beams are equal they will be in phase when returning to the beam splitter and will constructively interfere, appearing bright at the interferometer

---

*See Nomenclature for symbol definitions.

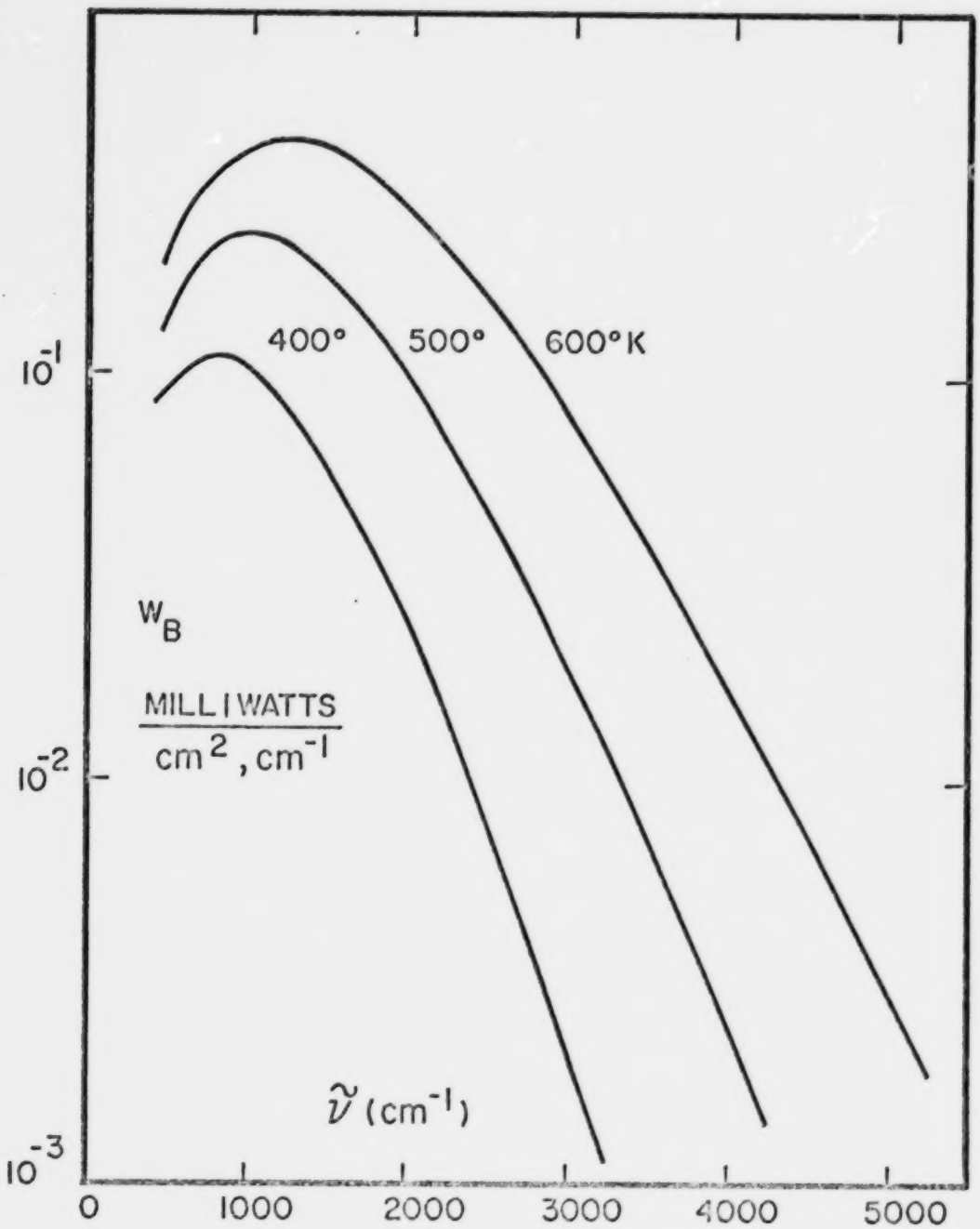

FIGURE 3 – BLACK BODY FUNCTION

output. Displacing the movable mirror $\lambda/4$ displaces the beams π radians out of phase, produces destructive interference making the field dark. Causing the mirror to move at a velocity $2B/\tau$ causes the flux transmitted by the interferometer to the detector to be,

$$J_d = \frac{f_o J}{2} \left[1 + \cos \left(\frac{4\pi B t}{\tau \lambda}\right) + \theta_\lambda\right] \tag{4a}$$

where the detector frequency is related to the radiation frequency by,

$$\nu_d = \left(\frac{2B}{\tau}\right)\frac{1}{\lambda} = \left(\frac{2B}{\tau}\right)\tilde{\nu} \tag{4b}$$

Then, $$J_d = \left(\frac{f_o A_m H}{2}\right)\left[1 + \cos \left(2\pi \nu_d t + \theta_\nu\right)\right] \tag{5}$$

which produces for the particular monochromatic radiation frequency an output from the detector (the interferogram) of,

$$u_d = \left(\frac{f_o A_m H}{2}\right)\mathcal{R}(\omega_d) \cos \omega_d t \tag{6a}$$

Actually for broad band radiation, rather than a single frequency, the detector voltage is complex, containing frequency components representing all radiation frequencies from the source; after conditioning and amplification the output voltage can be represented by,

$$U(t) = \left(\frac{G\, f_o\, A_m}{2}\right) \sum_{-\infty}^{\infty} H_i\, \mathcal{K}(\nu_{di})(\cos \omega_{di} t - j \sin \omega_{di} t) \qquad (6b)$$

From which in principle by Fourier Transformation, the frequency distribution function $S(\omega)$ can be obtained,

$$S(\omega_d) = \frac{1}{2\pi} \int_{\infty}^{\infty} U(t) e^{-j\omega_d t} dt \qquad (7a)$$

giving a set of intensities and frequencies,

$$S(\omega_d) = \{(Y_{\omega 1}, \omega_1), (Y_{\omega 2}, \omega_2), (Y_{\omega 3}, \omega_3) \ldots .\} \qquad (7b)$$

and converted into a set of values,

$$Y_{\tilde{\nu} i} = \alpha \left(\frac{G\, f_o\, A_m\, H_i\, \mathcal{K}_{\tilde{\nu} i}}{2}\right) \qquad (8a)$$

$$\tilde{\nu}_i = \left(\frac{\tau}{4\pi B}\right) \omega_{di} \qquad (8b)$$

TEMPERATURE MEASUREMENT - Total Energy Method.

The first most important quantity to be determined, when remotely sensing a hot body, is the temperature. Several methods were explored, but the most effective, reproducible and simplest proved to be the total energy method; wherein all component frequency intensities, over the spectral range (e.g., $\Delta\tilde{\nu}$ = 500 to 4000 cm^{-1}), are added together. At zero retardation of the interferometer mirrors all frequencies have the same phase and

add to give a measure of the total energy, as indicated by the maximum amplitude in the interferogram, and consequently a measure of the temperature of the observed body and the geometry.

Assume one is observing a hot gray body in vacuo, equations (2) and (8) can be combined to give,

$$\left(\frac{2Y}{\mathcal{K}GA_m X^2}\right) = \int_{\Delta\tilde{\nu}} \varepsilon_{\tilde{\nu}} W_{B\tilde{\nu}} d\tilde{\nu} = \varepsilon \overline{W}_B \Delta\tilde{\nu} \tag{9}$$

where Y is the total signal; then,

$$\left(\frac{2Y \cdot 10^4}{\mathcal{K}GA_m X^2 \varepsilon \Delta\tilde{\nu} \cdot 10^4}\right) = c_1 \bar{\tilde{\nu}}^3 \left(e^{\frac{c_2 \bar{\tilde{\nu}}}{T}} - 1\right)^{-1} \propto c_1 \bar{\tilde{\nu}}^3 e^{-\frac{c_2 \tilde{\nu}}{T}}$$

Defining a "normalized temperature signal, N_T" as,

$$N_T \equiv \left(\frac{2Y \cdot 10^4}{\mathcal{K}GA_m X^2 \varepsilon \Delta\tilde{\nu} c_1 \bar{\tilde{\nu}}^3}\right) = e^{\frac{-c_2 \bar{\tilde{\nu}}}{T}} \cdot 10^4 \tag{10}$$

which can be rearranged into the form,

$$\left(10 - \frac{1000}{T}\right) = 10 - \frac{4(2.303 \cdot 10^3)}{c_2 \bar{\tilde{\nu}}} + \left(\frac{2.303\ 10^3}{c_2 \bar{\tilde{\nu}}}\right) \log_{10} N_T \tag{11}$$

and letting the temperature function, $\eta \equiv \left(10 - \frac{1000}{T}\right)$ which has the advantage that as η increases T increases, gives a "generalized temperature function" for all classes of hot radiating bodies,

$$\eta = b + m \log_{10} N_T \tag{12}$$

When viewing a gray body the normalized temperature signal will be the sum of a continuous spectrum; whereas when viewing a hot combustion gas plume the species CO_2, CO, and H_2O will contribute primarily to the spectral content, and over an effectively less $\Delta\tilde{\nu}$.

POLLUTANT CONCENTRATION MEASUREMENT.

The concentration of a specific pollutant in the plume is by, $(y_i, \tilde{\nu}_i)$ over a small $\Delta\tilde{\nu}$, consequently equation (9) can be written,

$$\varepsilon_{\tilde{\nu}} = (1-e^{-k_{\tilde{\nu}}x}) = \left(\frac{2y}{\mathcal{K}GA_m X^2 \Delta\tilde{\nu}\overline{W}_B}\right) \tag{13}$$

since the concentrations are small. The exponential term can be expanded in a series, and the concentration of the component (in parts per million at 1.0 atm. total pressure) is given by,

$$C_{i\,(ppm)} = \frac{v_i \cdot 10^6}{V} = \frac{p_i \cdot 10^6}{P} = \left(\frac{2 \cdot 10^6 y}{k_{\tilde{\nu}} \ell \mathcal{K}_{\tilde{\nu}} GA_m X^2 \Delta\tilde{\nu}\overline{W}_{B\tilde{\nu}}}\right)_i \equiv N_{C_i} \tag{14a}$$

where the "normalized concentration signals, N_{C_i}" can be defined as the right hand member of the equation and is numerically equal to the concentration in ppm. If the concentration in micrograms/m^3

is desired (currently in use) then,

$$C_i\,(\mu g/m^3) = \left(\frac{M_i \cdot 10^3}{RT}\right) C_i \qquad (14b)$$

For purposes of this investigation we were primarily interested in the pollutants: CO, unburned (CH_4 plus higher parafins) and pyrolyzed hydrocarbon products (olefins), NO and NO_2, which are involved in thermal and photochemical reactions in the emerging plume and in the atmosphere. The infrared bands selected for identification of the components are indicated in Table I and shown in Figure 4; good laboratory absorption spectrograms are presented by Pierson, Fletcher, and St. Clair (1956).

As part of this project, Campani, Fang, and Prengle (1972) measured $k_{\tilde{\nu}}$-values, required for equation (14), for a number of pollutant gases over a wide range of optical path lengths, and fit the data by correlation functions; which for the concentration ranges involved can be represented by,

$$k_{\tilde{\nu}i} = A_i \left(\frac{T}{T_o}\right)^n x_i^q \qquad (15)$$

Values of the constants are given in Table II.

·TABLE I· SELECTED INFRARED BANDS·

Component	Band Chosen & Width	Band Description	References
CO	4.60μ $\Delta\tilde{\nu}\simeq 92$ cm^{-1} (2147→2239)	1) ν_1-vibrational rotational band, P&R branches 2) R-branch used, maximum at 2170 cm^{-1} approx.	(Herzberg, 1939) (Banwell, 1966) (Pierson, Fletcher et al, 1956)
NO	5.25μ $\Delta\tilde{\nu}\simeq 100$ cm^{-1} (1880→1980)	1) ν_1-vibrational rotational band, P&R branches 2) R-branch used, maximum at 1905 cm^{-1} approx.	(Pierson, Fletcher et al., 1956) (Smith, Keller et al, 1951)
CH_4 & other paraffins	7.65μ $\Delta\tilde{\nu}\simeq 105$ cm^{-1} (1275→1380)	1) ν_4-vibrational rotational (1306 cm^{-1}, multiplicity = 3) 2) C_2H_6, ν_2 = 1375, ν_6 = 1379 cm^{-1} 3) C_3H_8, ν_{12} = 1278, $\nu_{20}+\nu_{14}$ = 1338, ν_6=1370, ν_{18} = 1375 cm^{-1}	(Herzberg, 1945) (Pierson, Fletcher et al., 1956)
C_2H_4 & other olefins	10.1μ, 10.6μ $\Delta\tilde{\nu}$=60 cm^{-1} (940→1000)	1) ν_{10}, ν_7 vibrational rotational bands 2) C_3H_6, $\nu_{14}+\nu_{20}$ = 963, ν_{18} = 996 cm^{-1}	(Herzberg, 1945) (Pierson, Fletcher et al., 1956)
NO_2	12.65μ $\Delta\tilde{\nu}$=70 (780→850)	1) Combination bands	(Pierson, Fletcher et al., 1956)

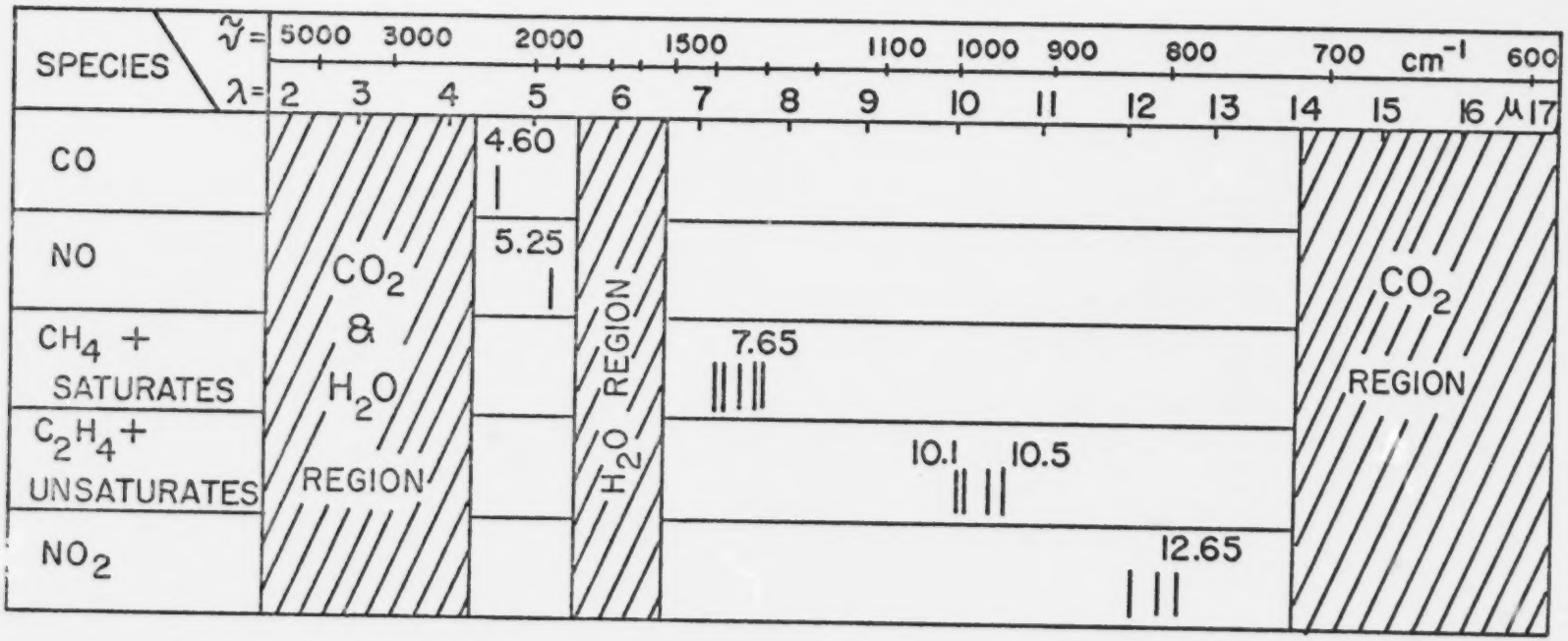

FIGURE 4 — POLLUTANT IDENTIFICATION FREQUENCIES

·TABLE II· CONSTANTS FOR ABSORPTION COEFFICIENT FUNCTIONS·

Component	A_i	T_o	n	q
CO (4.60μ, 2170 cm^{-1})	0.413	298.2	-1.00	-0.572
NO (5.25μ, 1905 cm^{-1})	0.374	297.8	-1.082	-0.594
CH_4 (7.65μ, 1308 cm^{-1})	1.940	297.8	-2.410	-0.813
C_2H_4 (10.1μ, 988 cm^{-1}) (10.52μ, 950cm^{-1})	1.508	297.8	-0.693	-0.556

LABORATORY & FIELD TESTS.

Initial measurement were made with the equipment using a 16.50 cm. dia. laboratory gray body viewed at distances of 3.58, 15.00, 24.60, 45.27 and 69.57 m., and at known temperatures of 375, 420, and 500°K to determine, distance factors, overall responsivity of the system, optimum operation of the equipment, and to check out the data processing programs.

Following these measurements, field tests were conducted viewing plumes from four power plant stacks, located at approximately 65 m. distance from the observation point. Figure 5 is a typical configuration of one stack, the emerging plume and the telescope field-of-view. During an observation period, direct measurements were made simultaneously of the plume temperature and pollutant concentrations.

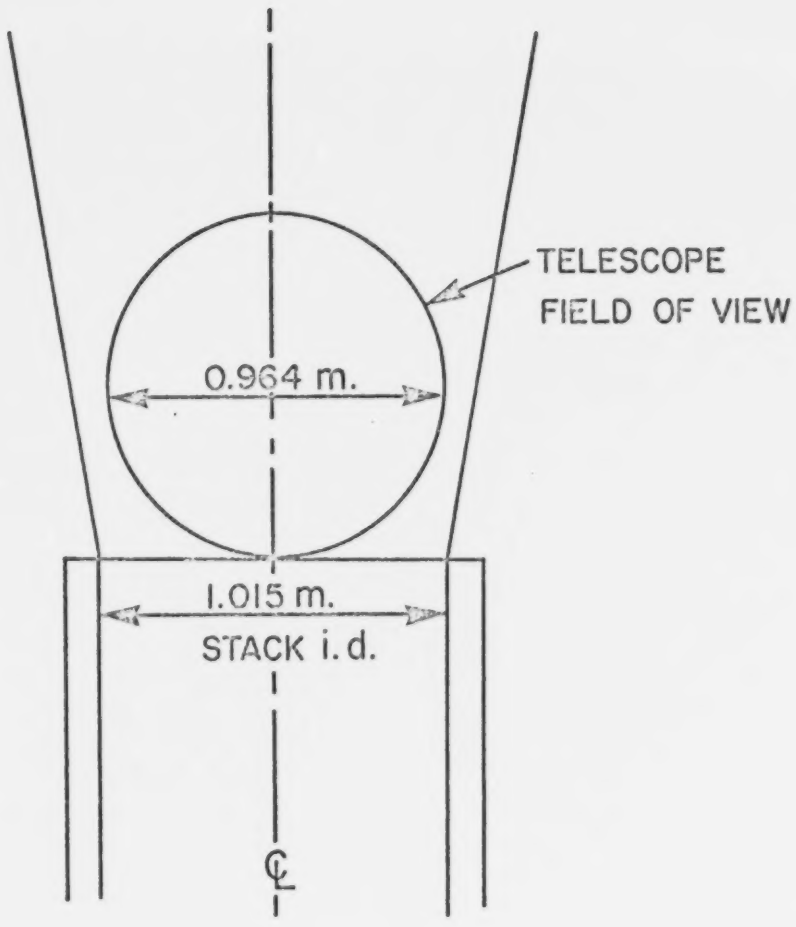

FIGURE 5 — PLUME FIELD-OF-VIEW
(POWER PLANT STACK NO. 1 , AT 65.70 m. DISTANCE)

A high methane sulfur free gas is burned in the power plant, Table III, gives a typical gas analysis. The stack gas was analyzed with a U.S. Bureau of Mines precision gas analyzer (Burrell Corp., 1951; U.S. Bureau of Mines, 1925) using standard absorbants (CO_2, KOH; O_2, $CrCl_2$; CO, oxidized to CO_2 over CuO; hydrocarbons oxidized to CO_2 over hot Pt-wire). NO_2 and NO were determined by the Saltzman method (1954), the NO being oxidized to NO_2. Typical analyses of the stack gases are also presented in Table III. It is interesting to note that even with excess oxygen the range of concentrations were: 1) CO = 2000 to 5000 ppm. 2) total hydrocarbon = 1000 to 2000 ppm. of which approximately 75% were saturates (C_1, C_2 and C_3) and 25% were olefins (C_2, C_3) by mass spectrometer analysis. 3) NO = 200 to 500 ppm. and NO_2 = 10-30 ppm.

RESULTS & CORRELATION.

The generalized temperature function is given by equation (12), and the normalized temperature signal by equation (10), which for equipment operational purposes becomes,

$$N_T = \left(\frac{10^4}{\mathcal{K} A_m \varepsilon \Delta\tilde{\nu} c_1 \bar{\nu}^3}\right)\left(\frac{2Y}{GX^2}\right) = a\left(\frac{S_m}{GF_o X^2}\right) \qquad (16)$$

·TABLE III· FUEL & STACK GAS ANALYSES·

-Fuel Gas*-		-Typical Stack Gas*-			
Component	v%	Component	Stack #1	Stack #4	Stack #1
O_2	nil	O_2	2.54	3.20	2.30
CO_2	0.44	CO_2	9.38	10.15	8.50
N_2	0.19	CO	0.513 (5130 ppm.)	0.400	0.347
CH_4	96.51	N_2+Ar^+	87.33	86.04	88.70
C_2H_6	2.27	total hydrocarbon	0.1900	0.1833	0.1170
C_3^+	0.59	CH_4+sats.	(1430 ppm.)≠	(1380 ppm.)	(880 ppm.)
Sp.Gv. 60°F	0.5778	C_2H_4+unsats.	(470 ppm.)≠	(453 ppm.)	(290 ppm.)
BTU/ft^3, 60°F	1015	NO	0.0473	0.0224	0.0376
		NO_2	0.0026	0.0027	0.0016
Total	100.00		100.00	100.00	100.00

*Dry basis ≠ By mass spectrometer analysis

+By difference

As a result of 20 temperature runs with the laboratory gray body, the system constants were determined and are given in Table IV; some parameters were fixed as a result of basic considerations whereas others (below the dotted line in the table) were evaluated from the experimental data. In addition 10 plume temperature runs were made, from which the average plume emissivity, ε, was determined. A plot of the generalized temperature function showing both gray body and plume temperature runs is presented as Figure 6.

A typical run consists of scanning the plume over the spectral range approximately every 3 sec. for a total of 20 to 100 scans. The peak signal monitor voltage at zero retardation, S_m is read for every scan and averaged for the total number of scans. Obviously the plumes involved will have turbulent temperature fluctuations and will be observed as fluctuations in S_m readings. The temperature fluctuations can be calculated from,

$$\delta T = \left(\frac{m' T_{avg}^2}{N_T}\right) \delta S_m \qquad (17)$$

obtained by differentiating equation (10). Three typical runs are shown as Figure 7, indicating fluctuations in the range of ±10°K,

·TABLE IV· SYSTEM PARAMETERS·

		Gray Body	Plume
$\tilde{\nu}$	(cm^{-1})	2000	=
$C_1\tilde{\nu}^3$	(milliwatts cm^{-1})	29.928	=
$\Delta\tilde{\nu}$	(cm^{-1})	3500	2750
ε	(1)	0.945	0.5233×10^{-2}
		L(m.)	
F_o	(1)	30.0 0.495	=
		40.0 0.720	=
		50.0 1.000	=
		70.0 1.540	=
$\mathcal{K}$	(volts milliwatts^{-1})	2.899×10^{-2}	=
$(\frac{\mathcal{K}_{\tilde{\nu}}}{\mathcal{K}})$	(1)	1.000	$\tilde{\nu}$=950 0.202
			1350 0.502
			1850 1.108
			2250 0.891
a	(volts^{-1})	0.7355×10^{-2}	1.233
m	(1)	0.93488	=
b	(1)	6.2605	=

$A_m = 475\ cm^2$

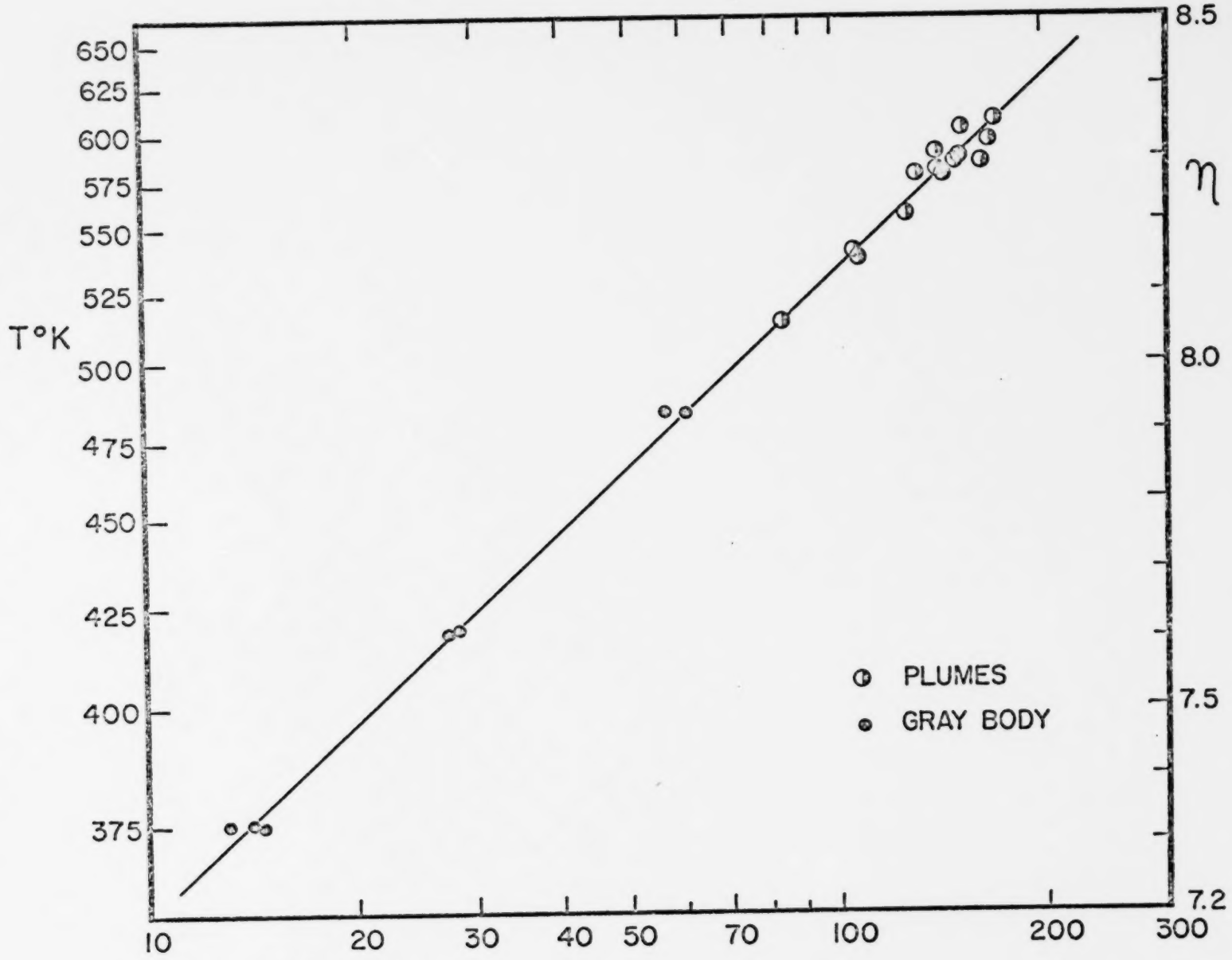

$$N_T \equiv \left(\frac{a\,S_m}{G\,F_o\,X^2}\right)$$

FIGURE 6 – GENERALIZED TEMPERATURE FUNCTION

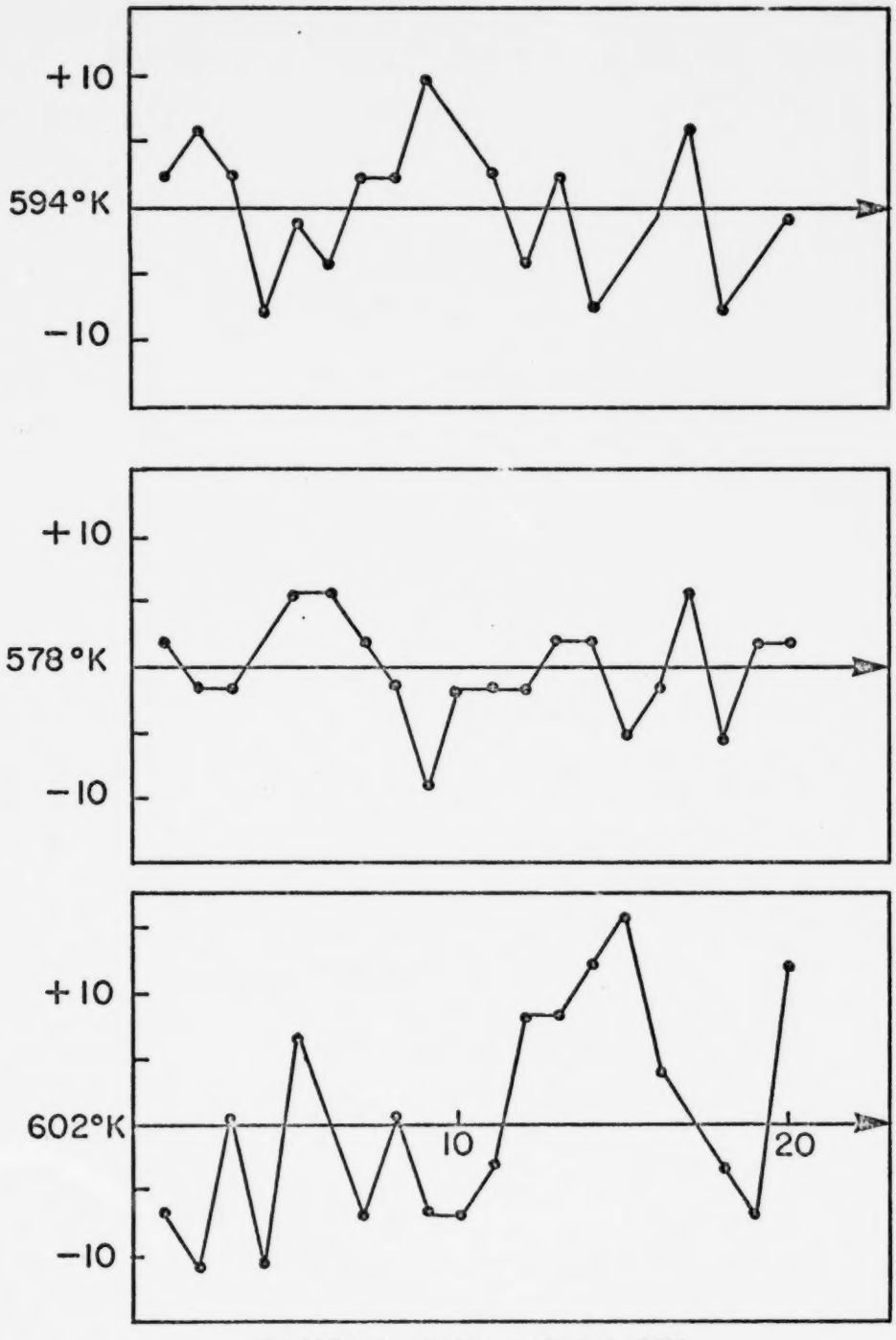

FIGURE 7 – TURBULENT TEMPERATURE FLUCTUATIONS

which is the magnitude one would expect from fluid dynamics considerations. We interpret these values to be real since they do not occur when viewing the laboratory gray body at comparable distances and temperatures.

The generalized concentration function is given by equation (14), and for equipment operational purposes becomes,

$$C_i = N_{Ci} \equiv \left(\frac{2 \cdot 10^6}{\ell G A_m F_o X^2}\right)\left(\frac{y}{k_{\tilde{\nu}} \mathcal{K}_{\tilde{\nu}} \Delta\tilde{\nu} W_{B\tilde{\nu}}}\right)_i \qquad (18)$$

where additionally the parameters $k_{\tilde{\nu}}$, $\mathcal{K}_{\tilde{\nu}}$ and $\Delta\tilde{\nu}$ are required in the determination of a particular pollutant concentration. The data from a series of 10 pollutant concentration runs were correlated by the generalized function, shown in Figure 8, and resulted in values of $(\mathcal{K}_{\tilde{\nu}}/\mathcal{K})$ given in Table IV. We estimate that, $\sigma = \pm 28\%$; i.e., 68% of the values fall within σ of the curve value. Data for a typical run showing determination of the plume temperature and pollutant concentrations, are presented in Table V; also indicating the extent of agreement with measured values.

The equipment can be maintained "in calibration" by a routine periodic measurement with a laboratory gray body and a sampled plume run.

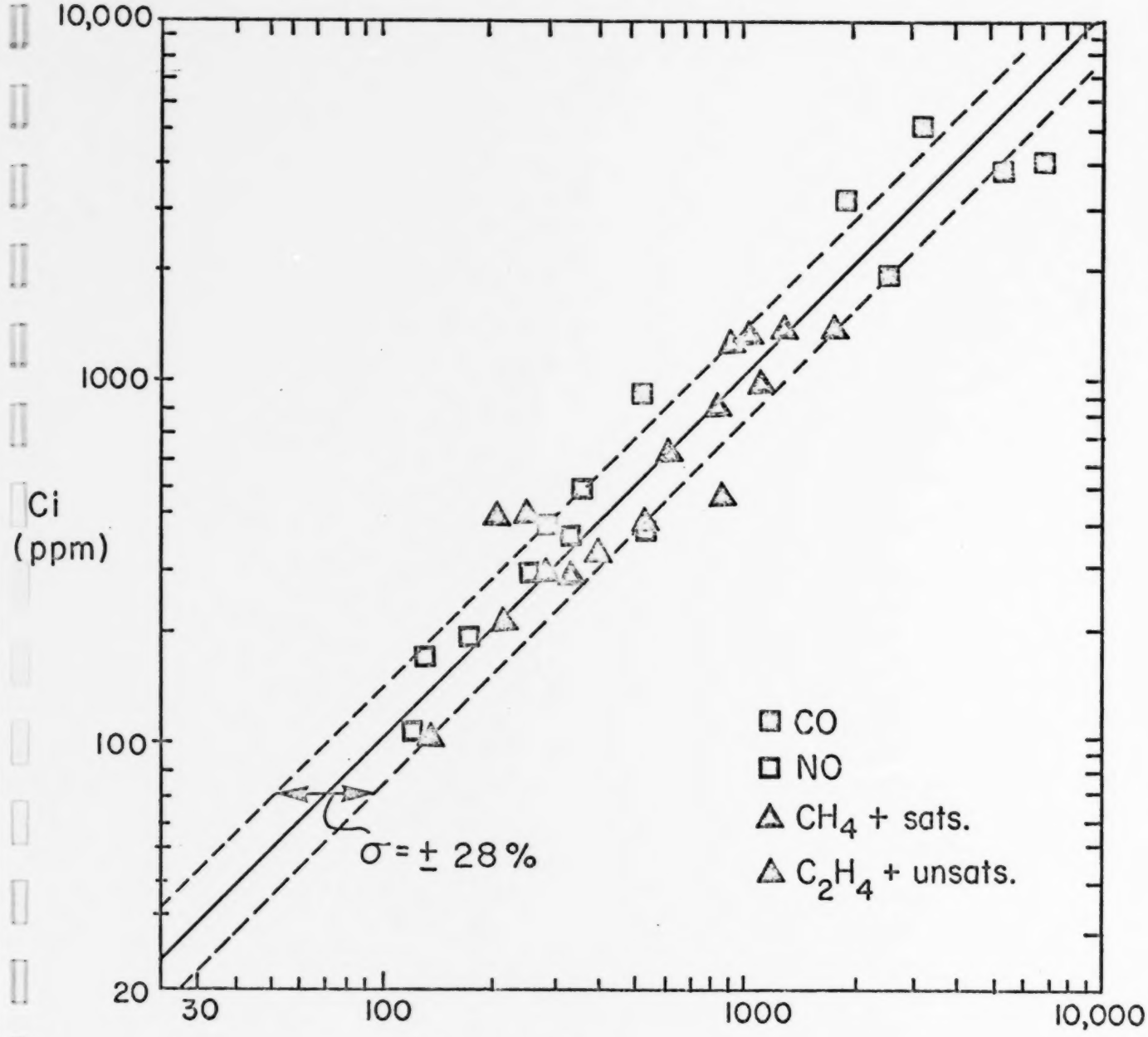

$$N_{Ci} \equiv \left(\frac{2 \times 10^6}{\ell_G A_m F_o X^2}\right)\left(\frac{y}{k\tilde{\nu}^R \tilde{\nu}^{\Delta\tilde{\nu}} W_{B\tilde{\nu}}}\right)_i$$

FIGURE 8 — GENERALIZED POLLUTANT FUNCTION

·TABLE V· TYPICAL RUN DATA·

r	0.614 m.		
ℓ	52.06 cm.		
L	67.19 m.	N_T	123.5
X^2	0.836×10^{-4}	η	8.217
F_o	1.43	T	560
G	350		
S_m	4.19	T(measured)	561

Components	CO	NO	CH_4+sats.	C_2H_4+unsats.
y	0.652	0.1960	1.016	0.2781
$k_{\tilde{\nu}}$	0.504	1.962	5.157	9.970
$\kappa_{\tilde{\nu}}$	3.45×10^{-2}	2.55×10^{-2}	1.43×10^{-2}	0.595×10^{-2}
$\Delta\tilde{\nu}$	100	100	100	100
$W_{B\tilde{\nu}}$	0.176	0.202	0.305	0.311
$N_C=C_i$	5500	524	858	296
C_i (measured)	4130 ppm	376 ppm	878 ppm	292 ppm

CONCLUSIONS.

1. A remote sensing radiometer spectrometer system, based on interferometer Fourier spectroscopy, for quantitatively determining pollutants in hot gas plumes has been developed and demonstrated to be feasible.

2. Generalized temperature and concentration models, based on theory with the inclusion of certain empirical factors, have been developed and their applicability demonstrated.

3. The pollutants: CO, NO and NO_2, unburned hydrocarbons, and combustion product olefins, have been quantatively determined.

The range can be extended to include oxidation products (e.g. aldehydes) produced in the plume reactor as it emerges into the atmosphere.

4. Measurements at distances up to 100 m. and for plume temperatures > 400°K are presently within the state-of-the-art, and with improved equipment (more sensitive detectors, etc.) and refined procedures, the range could be substantially extended.

5. Temperatures can be determined at 65 m. distance to ±10°K and concentrations to ±28% of the measured value over the range 10 to 10^4 ppm.; it appears that the error limits can be reduced.

6. The system can be used to observe temperature and concentration gradients as a plume emerges from its source. Also turbulent fluctuating temperature values can be determined within 0 to 10°K about a mean value, on a 1 to 3 sec. interval, and it appears possible to observe fluctuating pollutant concentrations.

7. Measurements on sulfur-free gas fired power plant indicate that typical concentration values are:

CO	2000 to 5000 ppm.
Total hydrocarbons	1000 to 2000 ppm. (approx. 75% saturates, 25% unsaturates)
NO	200 to 500 ppm.
NO_2	10 to 30 ppm.

This mixture along with excess oxygen (and from the atmosphere) and sunlight can produce other undesirable pollutant species.

NOMENCLATURE.

A_m	Area, telescope receiver mirror
B	1/2 of end-to-end optical retardation
C_i, C_{io}	Concentration, pollutant species "i"; and first approximation, respectively
F_o	Optical geometric and atmospheric factor
G	System gain
H	Irradiance of the receiver
J, J_d	Radiant flux, and transmitted to the detector respectively
L	Distance from receiver to plume
M	Molecular weight
N_C	Normalized concentration signal
N_T	Normalized temperature signal
R	Gas constant
$\mathcal{R}, \mathcal{R}_{\tilde{\nu}}$	Total responsivity, and spectral responsivity (at $\tilde{\nu}$) respectively
$S(\omega)$	Signal, frequency distribution function
S_m	Signal indicated by "signal monitor"
T, T_o	Temperature (°K), reference temperature respectively
U	Output voltage
V	Volume
X	r/L, dimensionless radius of the plume relative to the distance
Y	Total signal

Lower case.

a	System constant, defined by eqn. (16)
b	Constant in eqn. (12)

c	Velocity of light
c_1, c_2	Planck's black body constants $c_1 = 3.741 \times 10^{-9}$ milliwatts cm^2 $c_2 = 1.439$ cm•K
f_o	Optical factor
h	Planck's constant
k	Boltzmann's constant
$k_{\tilde{\nu}}$	Spectral absorption coefficient
ℓ	Path length in the plume
m	Constant in equation (12)
n	Slope of temperature function in $k_{\tilde{\nu}}$ correlation function
p	Partial pressure of pollutant species
r	Effective radius of plume in field of view
t	Time
u_d	Voltage output from detector
x	pl = effective optical path length
y	Spectral intensity signal

Greek•

α	scale factor
$\varepsilon, \varepsilon_{\tilde{\nu}}$	emissivity; and spectral emissivity or attenuation, respectively
η	dimensionless temperature function, $(10 - \frac{1000}{T})$
$\theta_\nu, \theta_\lambda$	phase angles
λ	wave length
$\nu_d, \tilde{\nu}$	detector frequency ; spectral frequency in wave numbers (cm^{-1}) respectively
σ	standard deviation
τ, τ_a	period; atmospheric transmission respectively
ω_d	detector angular frequency

ACKNOWLEDGMENT.

This investigation was supported by a research grant from the Air Pollution Control Office, Environmental Protection Agency. E.G. Felton assisted with the laboratory measurements.

LITERATURE CITED.

Anonymous, Environ. Sci. Tech. 5, 677 (1971).

Banwell, C.N., "Fundamentals of Molecular Spectroscopy", p. 75, McGraw-Hill, N.Y. (1966).

Block Engineering Co., Report: "FASFOR, A FORTRAN Program for Fourier Spectroscopy", (1967).

Block, L.C., Zachor, A.S., Appl. Opt. 3, 209 (1964).

Burrell Corporation, "Manual for Gas Analysts", 7th edition, (1951).

Campani, P., Fang, C.F., Prengle, H.W., Jr., Appl. Spectry. 26, March-April (1972).

Cooley, J.W., Tukey, J.W., Math. of Comput. 19, 297 (1965).

Dunn, S.T., Block, M.J., Amer. Lab., November (1969).

Dunn, S.T., Foskett, C.T., Ind. Res., 36, February (1971).

Hanel, R.A., Schlachman, B., Clark, F.D., Prokesh, C.H., Taylor, J.B., Watson, W.M., Chaney, L., Appl. Opt. 9, 1767 (1970).

Herzberg, G., "Molecular Spectra and Molecular Structure, I. Diatomic Molecules", Prentice-Hall, N.Y. (1939); "II. Infrared and Raman Spectra of Polyatomic Molecules", D. van Nostrand, N.Y. (1945).

Hochheiser, S., Burmann, F.J., Morgan, G.B., Environ. Sci. Tech., 5, 678 (1971).

Horlick, G., Appl. Spectry., 22, 617 (1968).

Lovett, J., Marcotte, L., Nadile, R., Report No., AFCL-67-0563, Office of Aerospace Research, USAF, (1967).

Low, M.J.D., J. Chem. Educ. 43, 637 (1966).

Low, M.J.D., Int. Sci. Tech. February (1967).

Low, M.J.D., Coleman, I., Spectrochim. Acta., 22, 369 (1966).

Martin, A.E., "Infrared Instrumentation and Techniques", Chapter 4, Elsevier Pub. Co., N.Y. (1966).

Mertz, L., Proc. 12th Intern. Astrophys. Symp. (Liege), U.S. Dept. of Commerce Report No., AD602936, p 120 (1963).

Pierson, R.H., Fletcher, A.N., St. Clair, G.E.,Anal. Chem., 28, 1218 (1956).

Rothschild, Lord, Proc. Roy. Soc. (London), A. 322, 147, (1971).

Saltzman, B.E., Anal. Chem., 26, 1949 (1954).

Smith, A.L., Keller, W.E., Johnson, H.L., J. Chem. Phys., 19 189 (1951).

U.S. Bureau of Mines, Tech. Paper No. 320 (1925).

Wark, D.Q., Appl. Opt. 9, 1761 (1970).

III. INFRARED ABSORPTION COEFFICIENTS FOR CERTAIN POLLUTANT GASES

by

P. Campani, C. S. Fang*, and H. W. Prengle, Jr.
Chemical Engineering Department, University of Houston
Houston, Texas (77004)

ABSTRACT

Quantitative analysis of gas mixtures by infrared spectroscopy requires a knowledge of the absorption coefficients, $k_{\tilde{\nu}}$, as a function of optical path length and temperature. For the majority of pollutant gases, information is scarce or incomplete. The objective of this work was to determine absorption coefficients for the following, CH_4, C_2H_4, CO_2, CO, SO_2, NO_2, NO, and H_2S. Measurements were made at room temperature and elevated temperatures for certain wavelengths, and $k_{\tilde{\nu}}$ determined over a very wide range of optical path length, x. The validity of the Bouguer-Beer law was confirmed for a limiting range of x, and for larger values of x, $k_{\tilde{\nu}}$ decreased and was correlated as a function of x and T.

Index headings: Infrared absorption coefficients; Pollutant gas IR absorption coefficients; Temperature effect on IR absorption coefficients.

July 1971
Revised October 1971

* Present address: Chemical Engineering Department, University of Southwestern Louisiana, Lafayette, La. (70501).

INTRODUCTION .

As part of a program to determine the concentrations of air pollutants in the atmosphere by long path absorption spectroscopy, and by remote emission spectroscopy, values of the infrared absorption coefficients for a number of pollutant gases were measured in our laboratory and are reported herein.

Infrared absorption coefficients can be determined by the Bouguer-Beer law[32]; for our purposes at constant temperature the transmittance τ can be written as,

$$\tau \equiv \frac{I}{I_o} = e^{-k_{\tilde{\nu}} p \ell} = e^{-k_{\tilde{\nu}} x} \qquad (1)$$

$$\ell n \frac{I_o}{I} = k_{\tilde{\nu}} x \qquad (2)$$

where, I, I_o = the resultant and incident intensities respectively (watts/cm^2)

$k_{\tilde{\nu}}$ = the monochromatic spectral absorption coefficient (atm^{-1}cm^{-1}) at $\tilde{\nu}$(cm^{-1})

p = the partial pressure (atm) of the absorbing gas

ℓ = the geometrical path length (cm)

$x = p\ell$ = the optical path length (atm.cm.)

If the law were valid for all values of x, $k_{\tilde{\nu}}$ would be constant and calculatable from experiments by,

$$k_{\tilde{\nu}} = \frac{1}{x} \ell n \frac{I_o}{I} \qquad (3)$$

A number of investigators[23,54] have reported in the literature that the Bouguer-Beer law is a limiting relationship, only valid for small values of the optical path length, x. A good discussion of the limitations is presented by Kortüm and

Seiler[23]. In most actual cases a plot of $\ell n\ I_o/I$ vs. x produces a curve which bends towards the x-axis as x increases; i.e. $k_{\tilde{\nu}}$ decreases as x increases.

A number of investigators have found that infrared band absorption falls off approximately as the square-root of the optical path length. Smith, Jones, and Chasmar[57] indicate that a square-root law should apply when,

1) the band is composed of unresolved lines of width less than the spacing, and/or

2) the path length is sufficient for most of the energy to be absorbed from the intense parts of the lines, residual absorption being due to overlapping tails in the spaces between the individual lines. A square-root law leads to,

$$\ell n\ k_{\tilde{\nu}} = C - 1/2\ \ell n\ x \tag{4}$$

and,

$$\text{slope} = \left(\frac{d\ \ell n\ k_{\tilde{\nu}}}{d\ \ell n\ x}\right) = -1/2 \tag{5}$$

The effect of temperature on absorption coefficients has been discussed by Breeze, Ferriso, Ludwig, and Malkmus[5] who proposed that the integrated intensity S(T) over $\Delta\tilde{\nu}$ could be represented by,

$$S(T) \equiv \int_{\Delta\tilde{\nu}} \frac{k_{\tilde{\nu}}}{p}\, d\tilde{\nu} = S(T_o)\left(\frac{T}{T_o}\right)^n \tag{6}$$

which in the limit as $\Delta\tilde{\nu} \to o$ gives

$$k_{\tilde{\nu}} = k_{\tilde{\nu}o}\left(\frac{T}{T_o}\right)^n \tag{7}$$

$$\ell n\ k_{\tilde{\nu}} = \ell n\ k_{\tilde{\nu}o} + n\ \ell n\ \frac{T}{T_o} \tag{8}$$

where, $k_{\tilde{\nu}}, k_{\tilde{\nu}o}$ = spectral absorption coefficients at absolute temperatures T and T_o respectively

T_o = reference temperature (°K), e.g. room temperature

n = constant, approximately -1.0

LITERATURE SEARCH

The characteristic frequencies for the gases of interest have been studied for years and are reported in numerous literature references. The most recent and complete surveys have been reported by Mavrodineanu and Boiteux[26]; Rao, Humphreys, and Rank[44]; the IUPAC[22]; and Herzberg[20].

A search of the literature was made for values of $k_{\tilde{\nu}}$ or data from which $k_{\tilde{\nu}}$ could be calculated; in general, information is scarce or incomplete; Table I presents a summary of the available data.

TABLE I • SUMMARY OF DATA FROM THE LITERATURE

Gas	Band Center cm^{-1} (μ)	Wavenumber Range, cm^{-1}	T °K	P atm	x cm-atm	Information Reported †
CO	2140(4.66μ)	1950-2300	300,600, 900,1000, 1200,1500, 2000,4000, 6000.	1/4,1/2 1,2, 3.	1,10,100, 1000,5,20, 40,60.	$\alpha_{\tilde{\nu}}$ vs $\tilde{\nu}$ $k_{\tilde{\nu}}$ vs $\tilde{\nu}$ $\varepsilon_{\tilde{\nu}}$ vs $\tilde{\nu}$
[Refs. 1,34,38,55]						
	4260(2.35μ)	3900-4400	297,1000, 2000,4000.	7/6		$k_{\tilde{\nu}}$ vs $\tilde{\nu}$
[Refs. 38,41,42,55]						
CO_2	667(15μ)	610-730	300,530, 1000,1390, 1520,1950, 2300.	6,8, 10.	0.0077,0.2063, 1.89,3.21	$k_{\tilde{\nu}}$ vs $\tilde{\nu}$ vs $\tilde{\nu}$ $\alpha_{\tilde{\nu}}$ vs $\tilde{\nu}$
[Refs. 9,18,25,47,52]						
	961(10.4μ)	850-1100	300,1500, 2300.	10.		$\alpha_{\tilde{\nu}}$ vs $\tilde{\nu}$
[Refs 27,28,34,47,52]						$\frac{I}{I_o}$ vs $\tilde{\nu}$
	2320(4.3μ)	2250-2400	300,600, 1273.		0.00455,0.455 1,10.	$\log \frac{I}{I_o}$ vs x S/d vs $\tilde{\nu}$ $\alpha_{\tilde{\nu}}$ vs $\tilde{\nu}$ $\varepsilon_{\tilde{\nu}}$ vs $\tilde{\nu}$
[Refs. 3,6,12,16,21,31,33,34,40,48]						
	3714(2.7μ)	3100-4200	1273	700/760	11.7	$\varepsilon_{\tilde{\nu}}$ vs $\tilde{\nu}$
[Refs. 15,34,50,56]						
	5109(1.96μ)	5000-5200	300	0.15,1.0, 10.	1490,330, 996	$\frac{I}{I_o}$ vs $\tilde{\nu}$
[Refs. 34,56]						

TABLE I continued

Gas	Band Center cm^{-1} (μ)	Wavenumber Range, cm^{-1}	T °K	P atm	x cm-atm	Information Reported
NO	1875.9(5.3μ)	1700-2000	273 3000,5000 7000,8000	500,365,210 psia	13,191, 206.	$\log \frac{I}{I_o}$ vs $\tilde{\nu}$ $\varepsilon_{\tilde{\nu}}$ vs $\tilde{\nu}$
[Refs. 5,8,35,46]						
	3751.8(2.7μ)	3000-4000	3000,5000 7000,8000		13,47.1 191,206,222	$\varepsilon_{\tilde{\nu}}$ vs $\tilde{\nu}$
[Ref. 35]						
NO_2	749.8(13.3μ)	650-1775	360	10^{-4}	3×10^{-3}	$\varepsilon_{\tilde{\nu}}$ vs $\tilde{\nu}$
[Ref. 8]						
	1318(7.59μ)					
	1618(6.19μ)	1520-1680	298	1.18	0.0584	$\log \frac{I}{I_o}$ vs $\tilde{\nu}$
[Ref. 17]						
	2220(4.5μ)					
	2908(3.44μ)	2860-2940	323	3.43	0.135,0.170, 0.257	$\log \frac{I}{I_o}$ vs $\tilde{\nu}$
[Ref. 17]						
N_2O_4	3442(2.9μ)	3300-3490	323	3.43	0.135,0.170 0.257,0.425	$\log \frac{I}{I_o}$ vs $\tilde{\nu}$
[Ref. 17]						
	3120(3.2μ)	3020-3170	323	3.43	0.135,0.170, 0.257,0.425	$\log \frac{I}{I_o}$ vs $\tilde{\nu}$
[Ref. 17]						

TABLE I continued

Gas	Band Center cm^{-1} (μ)	Wavenumber Range, cm^{-1}	T °K	P atm	x cm-atm	Information Reported
N_2O_4	2962(3.4μ)	2920-3010	323	3.43	0.135,0.170, 0.257,0.425	$\log \frac{I}{I_o}$ vs $\tilde{\nu}$
[Ref. 17]						
	1748(5.7μ)	1640-1820	298	1.18	0.0594	$\log \frac{I}{I_o}$ vs $\tilde{\nu}$
[Ref. 17]						
	1260(7.9μ)	1200-1300	298	1.18	0.0594	$\log \frac{I}{I_o}$ vs $\tilde{\nu}$
[Ref. 17]						
	750(13.3μ)	710-780	298	1.18	0.0594	$\log \frac{I}{I_o}$ vs $\tilde{\nu}$
[Ref. 17]						
NH_3	3448(2.9μ)	3100-3600	- not given -			$\log \frac{I}{I_o}$ vs $\tilde{\nu}$
[Refs. 4,30]						
	3337(3μ)	3100-3600	- not given -			$\log \frac{I}{I_o}$ vs $\tilde{\nu}$
[Refs. 4,30]						
	1628(6.15μ)	1300-2000	300	115.5/760 314/760 1630/760 687/760 3650/760	0.153 0.911	$\alpha_{\tilde{\nu}}$ vs $\tilde{\nu}$
[Ref. 13]						
	950(10.5μ)	700-1300	300	62.6, 467, 1310,4185 mm	0.0772, 1.617, 47.1	$\alpha_{\tilde{\nu}}$ vs $\tilde{\nu}$
[Ref. 13]						
SO_2	517.69(19.3μ)	450-625	360-420	1000 ppm	0.3	$\varepsilon_{\tilde{\nu}}$ vs $\tilde{\nu}$
[Ref. 8]						
	1151.38(8.68μ)	1000-1425	360-420	3000,1000	0.9,0.3	$\varepsilon_{\tilde{\nu}}$ vs $\tilde{\nu}$
[Ref. 8]						

TABLE I continued

Gas	Band Center cm^{-1} (μ)	Wavenumber Range, cm^{-1}	T °K	P atm	x cm-atm	Information Reported
SO_2	1361.76(7.35μ)			500 ppm	0.15	
[Ref. 8]						
	2295.88	2250-2520	360-420	10^{-4} atm	0.3	$\varepsilon_{\tilde{\nu}}$ vs $\tilde{\nu}$
[Ref. 8]						
H_2O	3710(27μ)	2900-4200	423,500, 1253	4.70, 1.23,1.31 1.44,3.10	7.26,2.34, 1.97,1.64, 1.37,1.12, 0.68,10.9, 60.8	$\varepsilon_{\tilde{\nu}}$ vs $\tilde{\nu}$
[Refs. 10,14,37,49,53]						
	1590(6.3μ)	1200-2200	540,1030, 1535,1850, 2150	1,1.23, 1.31,1.44, 3.10,2.54, 2.98,1.87	3.12,1.78, 6.92,16.3, 89.0	$\varepsilon_{\tilde{\nu}}$ vs $\tilde{\nu}$
[Refs. 24,53]						
	500(20μ)	500-1000	400,450, 500	2.	60.96	$k_{\tilde{\nu}}$ vs $\tilde{\nu}$
[Refs. 11,36,51]						
CH_4	4280(2.37μ)	3600-4600	295,669, 1138	780/760	7.72	$\alpha_{\tilde{\nu}}$ vs $\tilde{\nu}$
[Refs. 19,29,45]						
	3000(3.31μ)	2400-3400	295,669 1138	780/760	7.72	$\alpha_{\tilde{\nu}}$ vs $\tilde{\nu}$
[Refs. 19,29,45]						
	1310(7.65μ)	1050-1520	295,669 1084	780/760	7.72	$\alpha_{\tilde{\nu}}$ vs $\tilde{\nu}$
[Refs. 19,29,45]						

† where, $\alpha_{\tilde{\nu}} \equiv$ spectral absorptance; $\varepsilon_{\tilde{\nu}} \equiv$ spectral emissivity; S ≡ integrated intensity.

EXPERIMENTS CONDUCTED .

Data were obtained at ambient temperature for the following gases at the wave lengths and concentrations indicated:

CH_4	3.31μ	0.6 to 7 X 10^4 ppm. concentration
	7.65μ	0.3 to 7 X 10^4
C_2H_4	3.35μ	10^2 to 10^4
	10.12μ	20 to 10^3
	10.52μ	20 to 10^4
SO_2	4.01μ	10^3 to 10^4
	7.4μ	1. to 3 X 10^2
	8.6μ	1.5 X 10^2 to 4 X 10^3
NO_2	7.95μ	4 X 10^2 to 10^4
	12.65μ	10^3 to 10^4
NO	5.25μ	10^2 to 10^4
H_2S	7.75μ	3 X 10^4 to 5 X 10^5
CO	4.60μ	30 to 10^4
CO_2	4.26μ	5 to 3 X 10^2
	13.90μ	4 X 10^2 to 5 X 10^3
	15.00μ	5 to 3 X 10^2

and at elevated temperatures, up to 500°K.

C_2H_4 at	3.35μ	5 and 10 X 10^4
SO_2 at	4.01μ	1 and 5 X 10^5
CO_2 at	15.0μ	1 and 4.5 X 10^5

Nitrogen was used as the inert gas to give a total pressure of 1 atm. for all gas samples.

EXPERIMENTAL •

A. Apparatus

The equipment used in the experiments included, an evacuation system and loading rack, a double-beam spectrophotometer, a long path gas cell, and a heated gas cell.

The Gas Loading Rack consisted of, six measuring buretts, two mixing vessels, a two stage high capacity vacuum pump, a cold trap to remove condensibles, three precision pressure (vacuum) gauges, and a gas cylinder manifold with pressure regulators. The loading system was used to evaluate the infrared gas cells, and make up and charge gas mixtures of known composition for the experiments. Further details are presented elsewhere[7].

The Spectrophotometer used was a Perkin-Elmer Model 21, double beam, recording spectrophotometer. The monochromator has a 60° X 6 cm. base rock salt prism, with a working range of 2.0μ to 15.5μ. The instrument has, continuous variable speed scanning and recording of the transmittance (I/I_o) vs. a linear wave length scale; automatic or manual programming of the slit opening; and accuracy and reproducibility of ±0.05% in the 20-100% transmittance range and ±1.0% in the 0-20% range.

The long path cell, was a modified Perkin-Elmer 10-meter folded path cell designed to permit infrared measurements of low concentration gases. The path length of the cell can be adjusted from 1.25 m. up to 10.00 m. by means of an external micrometer. Two mirrors controlled by the micrometer rotate symmetrically varying the number of passes inside the cell from 4 to 32. The mirrors can be adjusted to give even greater path

length, but over 10 meters the astigmatism results in an energy loss which can be tolerated only in few applications. The external transfer optics permit the beam to be focused at the inlet window of the spectrophotometer. Since the transfer optics are normally exposed to the atmosphere, when working with gases or vapors also contained in the atmosphere (e.g. CO_2 and H_2O) it is necessary to use a cover over the cell cavity which can be continuously purged with dry nitrogen. The windows of the cell are of rock salt; the allowable pressure range of the cell is 50×10^{-3} to 7.6×10^{3} torrs.

The Heated Gas Cell used was a Beckman Model GH9 with a fixed path length of 9 cm and NaCl windows. Around the cell body a 120 watt electric coil provides necessary heat to attain temperatures up to 250°C. A valve is provided as a gas inlet and two ports with silicon rubber septa can be used to inject volatile liquids and for a thermocouple (iron-constantant) to measure the temperature.

Experimental measurements were made in accordance with procedures recommended by ASTM[2].

B. Calculation of $k_{\tilde{\nu}}$-Values

Laboratory spectrophotometers are energy limited, and finite slit widths must be used to pass sufficient radiation to operate the equipment; consequently a $k_{\tilde{\nu}}$ value obtained from the peak absorption will be the average value over the spectral slit width interval $\Delta\tilde{\nu}_s$, which for our prism monochromator is given by Potts[43] as,

$$\Delta\tilde{\nu}_s = \frac{\tilde{\nu}^2}{4\frac{dn}{d\lambda}}\left[\frac{S(1-n^2\sin^2\pi/12)^{1/2}}{27.0\sin\pi/12} + \frac{F(S)}{3\tilde{\nu}}\right] \quad (9)$$

where, $\Delta\tilde{\nu}_s$ = the minimum wave number interval which the monochromator can resolve

n = refractive index of the optical material

$\frac{dn}{d\lambda}$ = optical material dispersion

$F(S)$ = slit width function (0.90 to 0.50)

S = geometrical slit width (0.02 to 0.47 mm.)

Values for $\Delta\tilde{\nu}_s$ = 18.8 to 2.5 cm^{-1} for the range, $\tilde{\nu}$ = 3000 to 667 cm^{-1} were obtained for our experiments.

In an actual cell, energy is absorbed not only by the gas sample but also by the windows and mirrors; the I/I_o determined experimentally includes the sum effect of all attenuations. For a cell with 2 windows and 32 passes, mirror to mirror, these effects cannot be taken care of by simple subtraction; consequently a method must be devised to obtain the transmittance of the gas. A computer program was written which starts with I_o and stepwise calculates the attenuation of the beam as it passes through (or reflects from) all elements to obtain I; then τ_{calc} is compared to τ_{exptl} and when these values match after several iterations the correct value for τ_{gas} is obtained. The attenuation of the windows and mirrors is obtained from measurements on the empty cell and iterative calculations using the program. Details of the entire procedure are presented elsewhere[7].

C. Error Analysis

A detailed examination was made of the uncertainties in the calculated and correlated experimental values of $k_{\tilde{\nu}}$; the total

deviation being made up of deviations in the transmittance, partial pressure, and geometrical path length. Our best estimates indicate a standard deviation, $\sigma = 0.105$; i.e. 68% of the data fall within ±10.5% of the curve fit value.

RESULTS AND CORRELATION •

Typical plots of the data obtained are presented as Figures 1 and 2 for CO_2 at 15.0μ and 4.26μ and ambient temperature. Similar curves were obtained for all other substances examined. Also Figure 3 presents the effect of temperature for CO_2 at 15.0μ. Treatment of the data as a function of x and T indicated that the following correlation functions could be used:

Region 1 : $x < x_o$

$$\ell n\, k_{\tilde{\nu}} = \ell n\, k_{\tilde{\nu}o} + n\, \ell n(T/T_o) \qquad (10)$$

Region 2 : $x_o < x < x_1$

$$\ell n\, k_{\tilde{\nu}} = \ell n\, k_{\tilde{\nu}o} \left[\sum_{i=0}^{m} C_i (\ell n\, x)^i\right] + n\, \ell n(T/T_o) \qquad (11)$$

Region 3 : $x > x_1$

$$\ell n\, k_{\tilde{\nu}} = \ell n\, k_{\tilde{\nu}o} [C_o + C_1\, \ell n\, x] + n\, \ell n(T/T_o) \qquad (12)$$

Values for the constants, $\ell n\, k_{\tilde{\nu}o}$, n, T_o, C_o, C_1,.... in the above functions for the substances and respective frequencies are presented in Table 2. The constants were determined by least squares fit of the data.

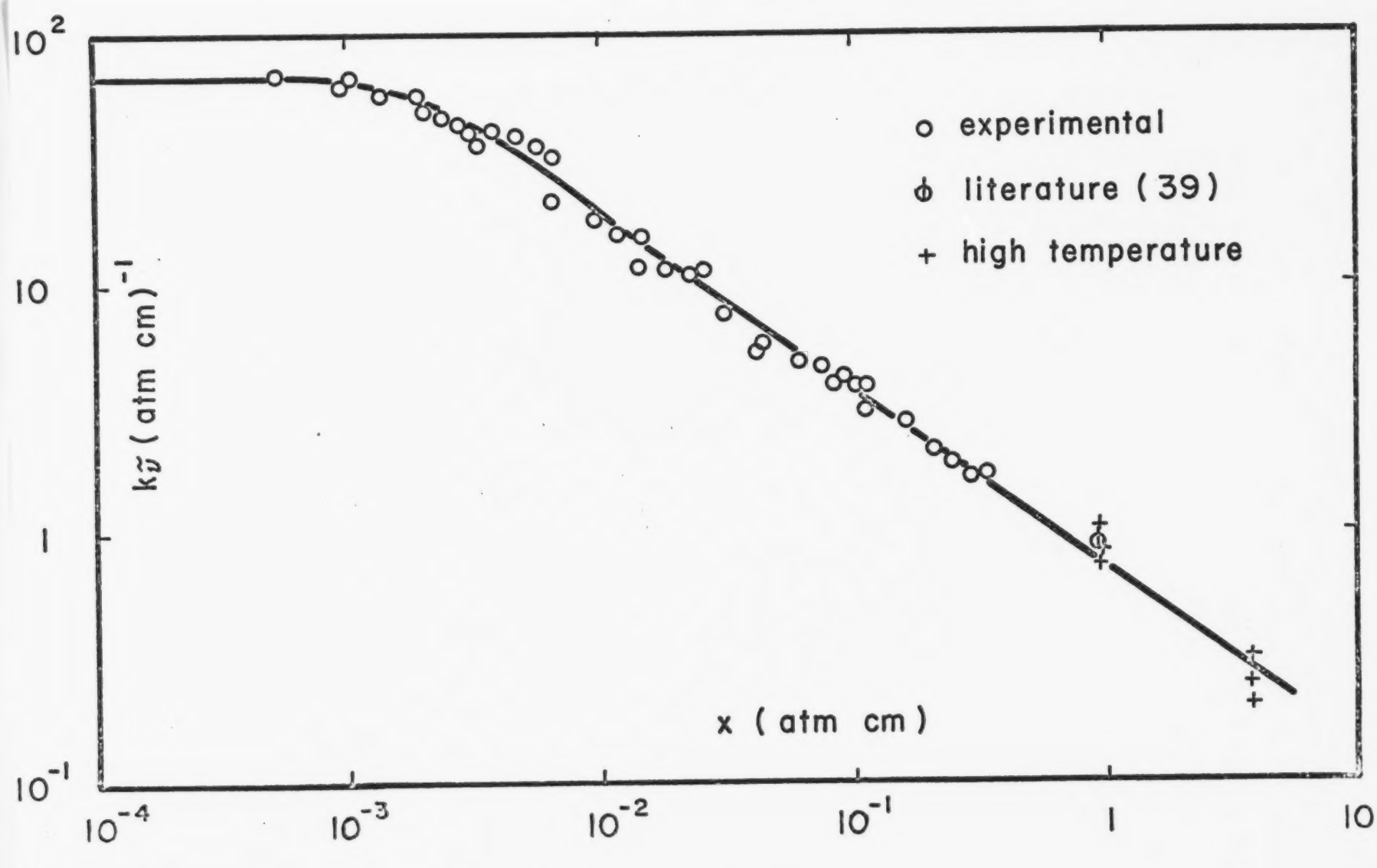

FIGURE 1 -- Carbon Dioxide at 15.0μ, T = 297.0°K

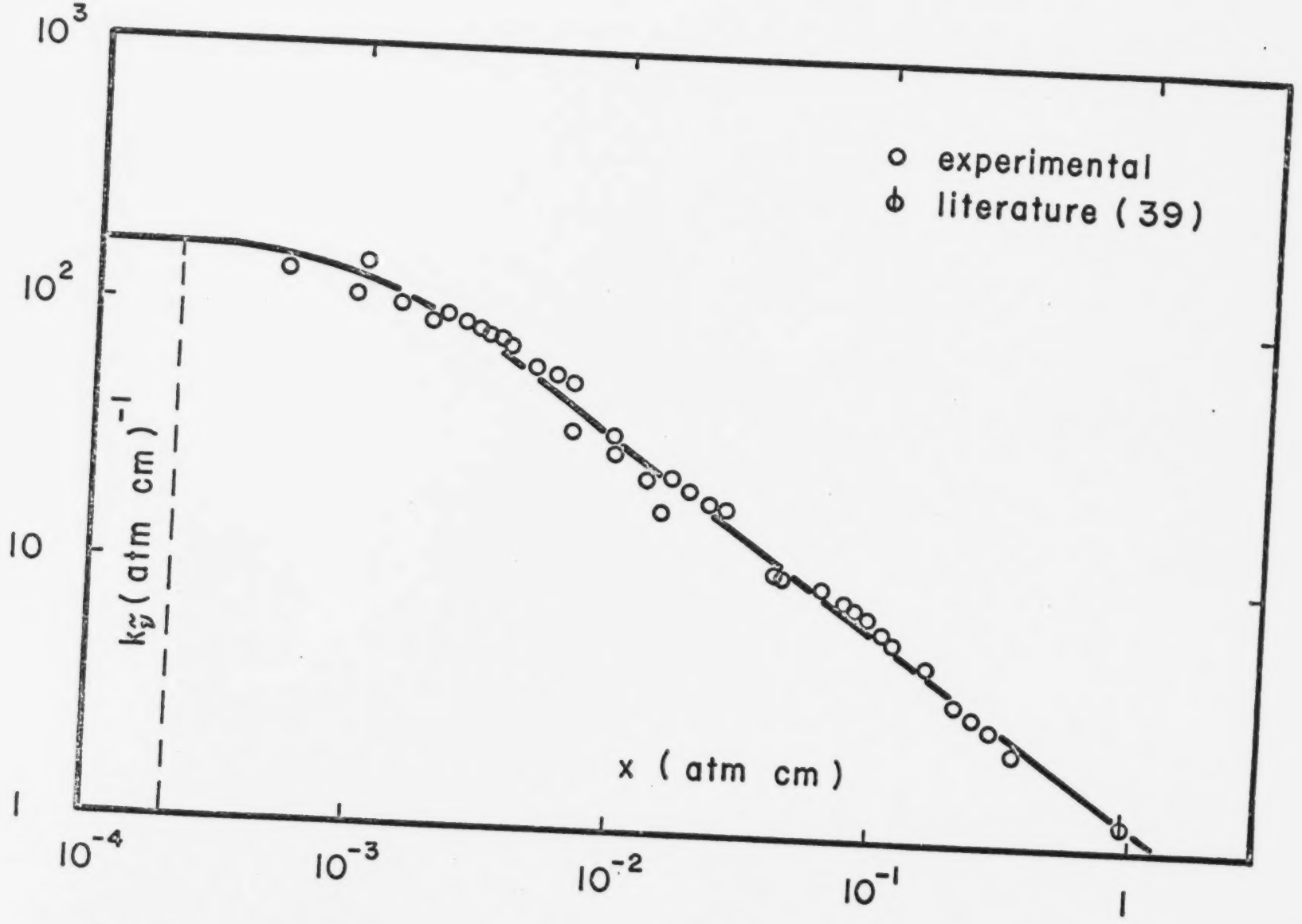

FIGURE 2 -- Carbon Dioxide at 4.26μ, T = 29.6°K

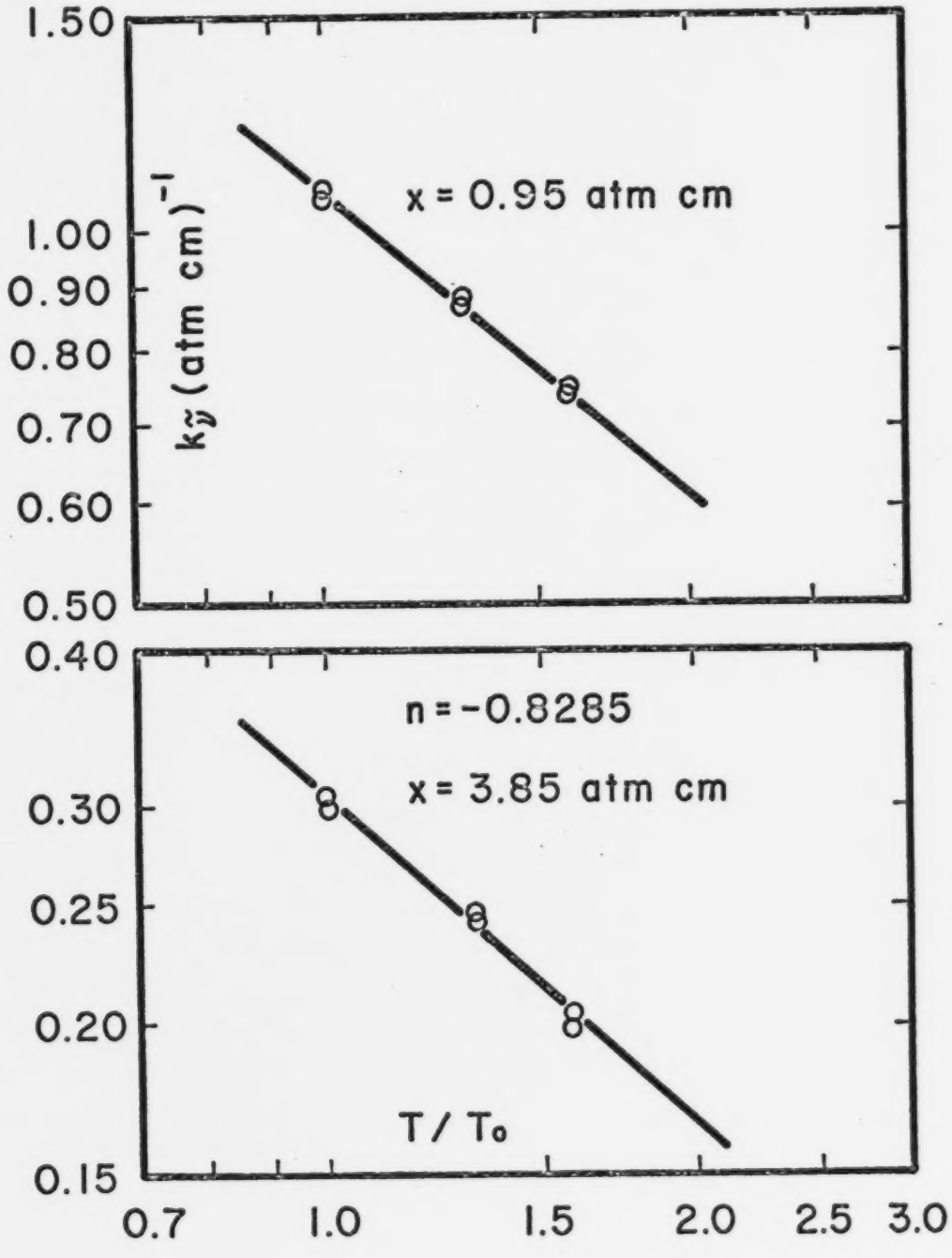

FIGURE 3 -- Temperature Effect, CO_2 at 15.0μ

TABLE II · CONSTANTS FOR CORRELATION FUNCTIONS

Substance	T_o x_o x_1 Np†	$k_{\tilde{\nu}o}$ ℓn $k_{\tilde{\nu}o}$ n	Region	C_o	C_1	C_2	C_3	C_4
CH_4	297.8	1736	2)	-0.03047	-0.1130	+0.01146	$+1.226\times10^{-3}$	---
7.65μ	0.8155×10^{-4}	7.4592						
1308 cm^{-1}	0.013	(-1.0)†	3)	0.08888	-0.1090			
$\Delta\tilde{\nu}_s$=4.8	150							
CH_4	297.9	2381	2)3)	-0.02923	-0.1042	1.740×10^{-4}	-2.732×10^{-3}	-6.766×10^{-4}
3.31μ	0.1755×10^{-4}	7.7754						
3020 cm^{-1}	---	(-1.0)						
$\Delta\tilde{\nu}_s$=18.8	76							
C_2H_4	297.6	1.670	2)	-1.301	-1.312	-0.1933	+0.1735	---
3.35μ	0.05501	0.5112	3)	-1.509	-1.053			
2990 cm^{-1}	2.175	-0.6926						
$\Delta\tilde{\nu}_s$=18.7	48							
C_2H_4	297.8	45.2	2)	0.03328	-0.2885	-0.7505	-0.01538	-1104×10^{-3}
10.12μ	0.1020×10^{-2}	3.8122						
988.1 cm^{-1}	0.2825×10^{-1}	(-0.6926)	3)	0.1079	-0.1461			
$\Delta\tilde{\nu}_s$=2.6	48							
C_2H_4	297.9	171.6	2)	0.06737	-0.1659	2.027×10^{-3}	1.022×10^{-3}	---
10.52μ	0.3224×10^{-3}	5.1451						
950.6 cm^{-1}	---	(-0.6926)						
$\Delta\tilde{\nu}_s$=2.6	47							

†Np ≡ number of data points ; ( ) ≡ estimated value

TABLE II - continued

Substance	T_o x_o x_1 Np	$k_{\tilde{\nu}o}$ ℓn $k_{\tilde{\nu}o}$ n	Region	C_o	C_1	C_2	C_3	C_4
CO_2	297.4	183.2	2)	0.09123	-0.07939	0.01918	1.874×10^{-3}	---
4.26μ	0.207×10^{-3}	5.2102						
2349 cm^{-1}	0.4633×10^{-1}	(-0.8285)	3)	0.06106	-0.1309			
$\Delta\tilde{\nu}_s$=13.6	40							
CO_2	297.1	3.07	2)	-0.7580	-0.3753	-0.02899	-0.03564	-6.321×10^{-3}
13.90μ	0.01151	1.121						
719.4 cm^{-1}	0.2981	(-0.8285)	3)	-0.8309	-0.4412			
$\Delta\tilde{\nu}_s$=2.0	28							
CO_2	297.0	67.3	2)	0.06717	-0.01947	+0.04740	$+4.459\times10^{-3}$	---
15.0μ	0.6862×10^{-3}	4.210						
666.7 cm^{-1}	0.04250	-0.8285	3)	-0.02889	-0.1567			
$\Delta\tilde{\nu}_s$=2.0	40							
CO	298.2	9.76	2)	-0.4373	-0.2512	3.802×10^{-3}	-8.256×10^{-3}	-1.565×10^{-3}
4.60μ	0.4083×10^{-2}	2.278						
2174 cm^{-1}	0.0923	(-1.0)	3)	-0.4357	-0.2856			
$\Delta\tilde{\nu}_s$=12.3	48							
SO_2	297.0	0.2105	2)3)	1.004	0.04096	0.2442	---	---
4.01μ	0.8244	-1.558						
2494 cm^{-1}	---	-1.358						
$\Delta\tilde{\nu}_s$=15.3	48							
SO_2	296.9	1322	2)	0.08429	-0.07031	+0.01507	1.298×10^{-3}	---
7.40	0.6647×10^{-4}	7.187						
1351 cm^{-1}	0.80×10^{-3}	(-1.358)	3)	0.05537	-0.1157			
$\Delta\tilde{\nu}_s$=5.2	48							

TABLE II - continued

Substance	T_o x_o x_1 Np	$k_{\tilde{\nu}o}$ ℓn $k_{\tilde{\nu}o}$ n	Region	C_o	C_1	C_2	C_3	C_4
SO_2	297.3	2.74	2)3)	-0.2220	-0.5859	-0.07026	---	---
8.60μ	0.01544	1.009						
1163 cm^{-1}	---	(-1.358)						
$\Delta\tilde{\nu}_s$=3.6	38							
NO_2	300.3	0.8768	2)3)	3.644	3.064	0.8877	---	---
7.95μ	0.1780	-0.1315						
1258 cm^{-1}	---	(-1.0)						
$\Delta\tilde{\nu}_s$=4.5	24							
NO_2	299.9	0.3182	2)3)	1.194	0.2471	0.07857	---	---
12.65μ	0.2075	-1.145						
791.8 cm^{-1}	---	(-1.00)						
$\Delta\tilde{\nu}_s$=2.0	32							
NO	297.8	2.35	2)	-1.096	-0.8325	-0.01437	+0.01573	---
5.25μ	0.02009	0.8559						
1905 cm^{-1}	1.693	(-1.00)	3)	-1.1495	-0.6944			
$\Delta\tilde{\nu}_s$=9.3	40							
H_2S	296.7	0.04217	2)3)	1.005	0.01943	0.02001		
7.75μ	0.6154	-3.166						
1290 cm^{-1}	---	(-1.00)						
$\Delta\tilde{\nu}_s$=4.8	32							

DISCUSSION

For long path absorption and emission spectroscopy of pollutants, where signals are weak, individual band spectra characteristics are needed which fall in the regions where water vapor does not interfere (approximately 3 - 5μ, and 7 - 15.5μ), and where the interference amongst the components is minimized. Individual component spectra might be vibrational, rotational or combinations thereof, whatever in the overall aspects suits operational criteria best. As a practical matter molecular collision effects at one atmosphere total pressure and resolution are such that band spectra are observed and not high resolution line spectra.

As a specific example consider carbon monoxide at 4.60μ (approx. 2170 cm^{-1}). A high resolution spectrum (gas pressure 100 mm. Hg abs.) covering the range 2020 - 2240 cm^{-1}, of the P and R rotational branches is presented by Banwell[58]. In the R-branch centered at approx. 2170 cm^{-1} (the band we measured), covering the range 2145 - 2240 cm^{-1} (band width 95 cm^{-1}), there are 28 rotational lines (R_0 to R_{28}) with a spacing of approx. 3-1/2 cm^{-1}. At higher pressure and resolution > 3-1/2 cm^{-1}, these lines merge together to produce the band spectrum observed by us and others[39], and presented in the well known paper by Penner and Weber[38]. To illustrate agreement with this reference the value of the maximum intensity of the band at p = 60 mm., ℓ = 6.22 cm., x = 0.491 atm. cm., T = 297°K, and P(total) = 15.0 psia., can be used to calculate the absorption coefficient,

$$k_{\tilde{\nu}} = \frac{1}{x} \ell n \frac{I_o}{I} = \frac{0.316}{0.491} = \underline{0.643 \text{ atm.}^{-1}\text{cm.}^{-1}}$$

and compared with the value from our correlation,

$$\ln k_{\tilde{\nu}} = 2.278[-0.4357-0.2856 \ln 0.491]-1.00 \ln \frac{297}{298.2}$$

$$= -0.5247 \; ; \; k_{\tilde{\nu}} = \underline{0.597 \pm 10\% \text{ atm.}^{-1}\text{cm.}^{-1}}$$

All factors considered one would expect $k_{\tilde{\nu}}$ - values to fall off for large values of x, perhaps according to the square-root law. The data indicate that the Bouguer - Beer law is satisfied for relatively short optical path lengths, but for larger values of x, $k_{\tilde{\nu}}$ decreases. It is interesting to compare the slopes, $(\frac{\partial \ln k_{\tilde{\nu}}}{\partial \ln x})_T$, given in Table III, to -1/2 predicted by the square-root law. It appears that the latter is a very rough approximation of the trend of actual data.

ACKNOWLEDGMENT ·

This investigation was supported by research grant AP00578, Air Pollution Control Office, Environmental Protection Agency. E. G. Felton assisted in the construction and calibration of the gas loading manifold and L. K. Huang conducted part of the literature search.

TABLE III - SLOPES cf. SQUARE - ROOT MODEL

Substance	Position	slope = C_1 ℓn $k_{\tilde{\nu}o}$
CH_4	7.65 μ	-0.812
	3.31	-0.811
C_2H_4	3.35	-0.538
	10.12	-0.557
	10.52	-0.853
CO_2	4.26	-0.681
	13.90	-0.494
	15.0	-0.658
CO	4.60	-0.652
SO_2	4.01	-0.638
	7.40	-0.830
	8.60	-0.591
NO_2	7.95	-0.403
	12.65	-0.283
NO	5.25	-0.713

LITERATURE CITED •

1. Abu-Romia, N. M., Tien, C. L., J. Quant. Spectrosc. Radiat. Transfer, 6, 143 (1966).

2. American Society for Testing & Materials; E168-67: "General Techniques of Infrared Analysis", third edition (1969).

3. Bahrov, Harold J., Tourin, Richard H., J. Quant. Spectrosc. Radiat. Transfer, 3, 15 (1963).

4. Benedict, W. S., Plyler, K., Tidwell, E. D., J. Chem. Phys. 32, 32 (1960).

5. Breeze, J. C., Ferriso, C. C., Ludwig, C. B., Malkmus, W., The J. Chem. Phys. 42, 402 (1965).

6. Burch, D. E., Gryvnak, D. A., J. Quant. Spectrosc. Radiat. Transfer, 6, 229 (1966).

7. Campani, P., M.S. Thesis, University of Houston; Houston, Texas (1971).

8. Dalmo Victor Company, "Final Report for Study of Infrared Techniques for Monitoring Stack Gases", PH86-65-61 (1965).

9. Edwards, D. K., Opt. Soc. Am. J., 50, 617 (1960).

10. Ferriso, C. C., Ludwig, C. B., J. Quant. Spectrosc. Radiat. Transfer, 4, 215 (1964).

11. Ferriso, C. C., Ludwig, C. B., Thomson, A. L., J. Quant. Spectrosc. Radiat. Transfer, 6, 241 (1966).

12. Ferriso, C. C. Ludwig, C. B., Acton, L., Opt. Soc. Am. J. 56, 171 (1966).

13. France, L., Williams, D., Opt. Soc. Am. J., 56, 70 (1966).

14. Goldstein, R., J. Quant. Spectrosc. Radiat. Transfer, 3, 91 (1963).

15. Gordon, R., McCubbin, T. K., Jr., J. Mol. Spectrosc. 19, 137 (1966).

16. Gray, L. D., J. Quant. Spectrosc. Radiat. Transfer, 5, 569 (1965).

17. Guttman, A., J. Quant. Spectrosc. Radiat. Transfer, 2, 1 (1961).

18. Harward, C. N., Patty, R. R., Opt. Soc. Am. J., 58, 188 (1968).

19. Herranz, J., Marcillo, J. Gomez, A., J. Molecular Spectrosc., 19, 266 (1966).

20. Herzberg, G., Infrared and Raman Spectra of Polyatomic Molecules, D. Van Nostrand (1945).

21. Hodgson, J. P., A Survey of the Infrared Radiation Properties of Carbon Dioxide, London (1968).

22. International Union of Pure and Applied Chemistry, "Tables of Wavenumbers for the Calibration of Infrared Spectrometers", Butterworth (1961).

23. Kortüm, G., Seiler, M., Angew. Chem. 52, 687 (1939). English translation No. 59-151-48, National Translations Center, John Crerar Library, Chicago, Ill.

24. Ludwig, C. B., Ferriso, C. C., Abeyta, C. N., J. Quant. Spectrosc. Radiat. Transfer, 5, 1537 (1968).

25. Ludwig, C. B., Ferriso, C. C., Acton, L., Opt. Soc. Am. J., 56, 1685 (1966).

26. Mavrodineanu, R., Boiteux, H., Flame Spectroscopy, Pt. II, 334, Wiley (1965).

27. McCubbin, T. K., Mooney, T. R., J. Quant. Spectrosc. Radiat. Transfer, 8, 1255 (1968).

28. McCubbin, T. K., Darome, R., Sorrell, J., Appl. Phys. Lett., 8 (1966).

29. McDowell, R. S., J. Mol. Spectrosc., 21, 280 (1966).

30. McKean, D. C., Schatz, P. N., J. of Chem. Phys. 24, 316 (1956).

31. Megill, L. R., Jamnick, P. M., Opt. Soc. Am. J., 51, 102 (1961).

32. Mellon, M. G., editor. Analytical Absorption Spectroscopy, J. Wiley and Sons, Inc. (1950).

33. Oppenheim, V. P., Ben-Aryeh, H., Opt. Soc. Am. J., 56, 171 (1966).

34. Penner, S. S., Olfe, D. B., Radiation and Reentry, Academic Press, New York (1968).

35. Penner, S. S., Sulzmann, K. G. P., Ludwig, C. B., J. Quant. Spectrosc. Radiat. Transfer, 1, 96 (1960).

36. Penner, S. S., Varanasi, P., J. Quant. Spectrosc. Radiat. Transfer, 7, 687 (1967).

37. Penner, S. S., Varanasi, P., J. Quant. Spectrosc. Radiat. Transfer, 5, 391 (1965).

38. Penner, S. S., Wever, D., The J. Chem. Phys. 19, 807 (1951).

39. Pierson, R. H., Fletcher, A. N., St. Clair. G. E., Anal. Chem., 28, 1218 (1956).

40. Plass, Gilbert N., Opt. Soc. Am. J., 49, 821 (1959).

41. Plyler, Earie K., Benedict, W. S., J. Chem. Phys. 20, 175 (1952).

42. Plyler, E. K., Blaine, L. R., Tidwell, E. D., J. Research N.B.S., 55, 183 (1955).

43. Potts, W. J. Jr., Chemical Infrared Spectroscopy, Vol. I, Wiley, (1963).

44. Rao, K. N., Humphreys, C. J., Rnak, D. H., Wavelength Standards in the Infrared, Academic Press (1966).

45. Rank, D. H., Eastman, D. P., Skorinko, G., Wiggins, T. A., J. Mol. Spectrosc., 1, 78 (1960).

46. Schurin, B., Clough, S. A., J. of Chem. Phys. 38, 1855 (1962).

47. Tourin, R. H., Appl. Opt. 2, 113 (1963).

48. Tourin, R. H., Opt. Soc. Am. J., 51, 175 (1961).

49. Tourin, R. H., Opt. Soc. Am. J., 51, 1225 (1961).

50. Tourin, R. H., Opt. Soc. Am. J., 51, 800 (1961).

51. Varanasi, P., Chou, S., Penner, S. S., J. Quant. Spectrosc. Radiat. Transfer, 8, 1537 (1968).

52. Varanasi, P., Lauer, J. L., J. Quant. Spectrosc. Radiat. Transfer, 6, 127 (1966).

53. Weiner, M. M., Edwards, D. K., Int. J. Heat Mass Transfer, 11, 55 (1968).

54. Willard, H. H., Merritt, L. L. Jr., Dean, J. A., Instrumental Methods of Analysis, 4th edition, D. Van Nostrand Co., Inc. (1965).

55. Young, L. A., J. Quant. Spectrosc. Radiat. Transfer, 8, 693 (1968).

56. Zachor, A. S., J. Quant. Spectrosc. Radiat. Transfer, 8, 1341 (1968).

57. Smith, R. A., Jones, F. E., Chasmar, R. D., The Detection and Measurement of Infrared Radiation, Oxford Univ. Press (1960).

58. Banwell, C. N., Fundamentals of Molecular Spectroscopy, McGraw-Hill (1966).

APPENDICES

APPENDIX A. TEMPERATURE RUNS.

1. Gray Body Temperature Runs.

Run	T°K η	r (cm)	L (m)	X^2	S_m	Fo	G	$N_T = \left(\frac{0.7335 \times 10^{-2} S_m}{Fo\ G\ X^2}\right)$
29	375 7.333	16.50	3.58	2.122×10^{-3}	3.0	0.0233	30	14.84
30	419 7.613	"	"	"	5.5	"	"	27.20
31	484 7.934	"	"	"	2.7	"	10	40.06
32	375 7.333	"	24.60	4.49×10^{-5}	2.9	0.377	100	12.57
"	375 7.333	"	"	"	9.9	"	350	12.26
33	419 7.613	"	"	"	6.3	"	100	27.30
34	484 7.934	"	"	"	3.9	"	30	56.33
35	484 7.934	"	"	"	4.2	"	"	60.67
36	375 7.333	"	15.00	1.21×10^{-4}	4.0	0.189	100	12.83
37	419 7.613	"	"	"	8.5	"	"	27.26
"	419 7.613	"	"	"	2.4	"	30	25.66
38	484 7.934	"	"	"	5.15	"	"	55.06
40A	375 7.333	"	45.27	1.33×10^{-5}	2.20	0.851	100	14.26
40B	375 7.333	11.48	45.27	0.668×10^{-5}	4.65	0.851	350	17.14
41A	419 7.613	16.50	"	1.33×10^{-5}	4.20	"	100	27.22
41B	419 7.613	11.48	"	0.668×10^{-5}	2.60	"	"	33.55
42A	484 7.934	16.50	"	1.33×10^{-5}	7.10	"	"	46.01
42B	484 7.934	11.48	"	0.668×10^{-5}	4.20	"	"	54.19
43	419 7.613	16.50	69.57	0.562×10^{-5}	3.20	1.532	"	27.26
44	484 7.934	"	"	"	5.25	"	"	44.73

1. Gray Body Temperature Runs. Continued

Run	T°K η	r (cm)	L (m)	X^2	S_m	Fo	G	$N_T = \frac{0.5364 \times 10^{-2} S_m}{Fo\ G\ X^2}$
57	419 7.613	16.50	25.95	4.0424×10^{-5}	8.50	0.40	100	28.20
63	419 7.613	"	25.47	4.1964×10^{-5}	8.80	0.395	100	28.50

2. Plume Temperature Runs.

Run	T°K η	r (m)	L (m)	X^2	S_m	G Fo	$N_T = \left(\frac{1.686\ S_m}{Fo\ G\ X^2}\right)$
39	589 8.302	0.603	65.97	0.837×10^{-4}	3.80	350 1.43	153.0
45	573 8.255	"	65.70	0.842×10^{-4}	4.25	350 1.43	170.0
46	594 8.316	"	65.97	0.837×10^{-4}	4.13	350 1.44	165.3
47	500 8.00	"	66.15	0.832×10^{-4}	2.66	350 1.44	107.0
48	562 8.221	0.656	66.39	0.975×10^{-4}	2.46	350 1.45	83.80
49A	578 8.270	0.604	66.09	0.834×10^{-4}	3.65	350 1.43	14.72
49B	602 8.339	0.610	67.66	0.813×10^{-4}	3.82	350 1.48	153.0
49C	500 8.00	0.618	69.82	0.784×10^{-4}	2.68	350 1.53	107.7
49D	575 8.261	0.684	73.43	0.868×10^{-4}	1.92	350 1.62	65.70
50	580 8.276	0.607	66.09	0.842×10^{-4}	4.02	350 1.43	162.1
51	580 8.276	0.605	66.09	0.837×10^{-4}	3.90	350 1.43	157.1

2. Plume Temperature Runs. Continued

Run	T°K η	r (m)	L (m)	X^2	S_m	G Fo	$N_T = \left(\frac{1.2329\ S_m}{Fo\ G\ X^2}\right)$
52	585 8.291	0.604	66.06	0.8359×10^{-4}	4.965	350 1.43	146.3
53	585 8.291	0.603	65.91	0.8385×10^{-4}	5.37	"	157.8
54	580 8.276	0.604	65.98	0.8385×10^{-4}	4.67	"	137.2
58	578 8.270	0.600	65.46	0.8390×10^{-4}	4.31	"	126.5
59	589 8.302	0.616	67.36	0.8359×10^{-4}	4.45	"	131.1
60	561 8.217	0.614	67.19	0.8359×10^{-4}	4.19	"	123.5
61	588 8.299	0.605	66.09	0.8385×10^{-4}	4.62	"	135.7
62	597 8.325	0.602	65.76	0.8390×10^{-4}	5.385	"	158.1

APPENDIX B° POLLUTANT CONCENTRATION RUNS.

1. CO ($\tilde{\nu}$=2200-2300, $\Delta\tilde{\nu}$=100)*

Run No. $\tilde{\nu}$(cm^{-1})	y' ℓ(cm)	I_{pp}	C_i(ppm) =p_i(atm) x10^6	x_i	$k_{\tilde{\nu}}$ W_B	y= $(\frac{y'S_m}{2\pi I_{pp}})$	$\mathcal{K}_{\tilde{\nu}}$	$\frac{\mathcal{K}_{\tilde{\nu}}}{\mathcal{K}}$	N_C= $[\frac{6.667\times10^4 y}{k_{\tilde{\nu}}\Delta\tilde{\nu}W_B(\mathcal{K}_{\tilde{\nu}}/\mathcal{K})_a}]$
50 $\tilde{\nu}$=2247	0.613 52.60	3.41	400	0.0210	1.934 0.159	0.1151	1.782 x10^{-2}	0.615	280
51 $\tilde{\nu}$=2259	0.775 52.11	3.51	900	0.0469	1.221 0.159	0.1369	1.516 x10^{-2}	0.523	528
58 $\tilde{\nu}$=2272	1.716 52.04	2.77	1933	0.1006	0.793 0.154	0.425	3.478 x10^{-2}	1.200	2604
59 $\tilde{\nu}$=2249	2.456 52.06	2.67	4130	0.2150	0.504 0.176	0.652	3.450 x10^{-2}	1.190	5500
60 $\tilde{\nu}$=2239	0.905 52.06	2.26	3470	0.1810	0.584 0.176	0.267	1.451 x10^{-2}	0.501	1944
61 $\tilde{\nu}$=2255	1.426 52.03	2.94	5133	0.2670	0.446 0.160	0.357	1.883 x10^{-2}	0.650	3743
62 $\tilde{\nu}$=2257	2.720 52.03	2.85	4200	0.2185	0.493 0.169	0.818	4.516 x10^{-2}	1.558	7347

*Values of r, L, X^2, S_m, G, F_o appear in Appendix A.

2. NO ($\tilde{\nu}$ = 1800 - 1900, $\Delta\tilde{\nu}$ = 100)

Run No. $\tilde{\nu}(cm^{-1})$	y' ℓ(cm)	I_{pp}	C_i(ppm) $=p_i$(atm) $x10^6$	x_i	$k_{\tilde{\nu}}$ W_B	$y=\left(\frac{y'S_m}{2\pi I_{pp}}\right)$	$\mathcal{R}_{\tilde{\nu}}$	$\frac{\mathcal{R}_{\tilde{\nu}}}{\mathcal{R}}$	$N_C=\left[\frac{6.667x10^4 y}{k_{\tilde{\nu}}\Delta\tilde{\nu}W_B(\mathcal{R}_{\tilde{\nu}}/\mathcal{R})_a}\right]$
52	0.835	3.01	298	0.0155	2.133	0.2194	2.822	0.974	261
$\tilde{\nu}$=1881	52.06				0.237		$x10^{-2}$		
53	0.685	3.04	104	0.00541	4.009	0.1927	3.770	1.300	122
$\tilde{\nu}$=1881	52.03				0.237		$x10^{-2}$		
54	0.902	3.15	130	0.00676	3.550	0.2129	3.763	1.298	166
$\tilde{\nu}$=1881	52.03				0.237		$x10^{-2}$		
58	0.706	2.77	194	0.01009	2.796	0.175	2.783	0.960	168
$\tilde{\nu}$=1917	52.04				0.224		$x10^{-2}$		
60	0.664	2.26	376	0.0196	1.962	0.1960	2.549	0.879	324
$\tilde{\nu}$=1881	52.06				0.202		$x10^{-2}$		
61	0.949	2.94	473	0.0246	1.701	0.238	2.413	0.832	355
$\tilde{\nu}$=1863	52.03				0.237		$x10^{-2}$		
62	1.446	2.85	389	0.0202	1.793	0.435	4.385	1.513	531
$\tilde{\nu}$=1863	52.03				0.2749		$x10^{-2}$		

3. CH_4 ($\tilde{\nu}$=1300-1400, $\Delta\tilde{\nu}$=100)

Run No. $\tilde{\nu}(cm^{-1})$	y' ℓ(cm)	I_{pp}	C_i(ppm) $=p_i$(atm) $x10^6$	x_i	$k_{\tilde{\nu}}$ W_B	y= $\left(\frac{y'S_m}{2\pi I_{pp}}\right)$	$\mathcal{K}_{\tilde{\nu}}$	$\frac{\mathcal{K}_{\tilde{\nu}}}{\mathcal{K}}$	N_C= $\left[\frac{6.667x10^4 y}{k_{\tilde{\nu}}\Delta\tilde{\nu}W_B(\mathcal{K}_{\tilde{\nu}}/\mathcal{K})_a}\right]$
52 $\tilde{\nu}$=1294	3.670 52.06	3.01	650	0.0338	5.982 0.341	0.9635	1.408 $x10^{-2}$	0.486	627
53 $\tilde{\nu}$=1294	4.456 52.03	3.04	998	0.0519	4.214 0.341	1.2528	1.688 $x10^{-2}$	0.582	1158
54 $\tilde{\nu}$=1294	4.206 52.03	3.15	308	0.01603	11.257 0.341	0.9924	1.622 $x10^{-2}$	0.560	343
58 $\tilde{\nu}$=1294	3.451 52.04	2.77	1250	0.0650	3.622 0.336	0.8546	1.085 $x10^{-2}$	0.374	933
59 $\tilde{\nu}$=1294	3.572 52.06	2.67	1298	0.0676	3.354 0.359	0.9475	1.175 $x10^{-2}$	0.405	1045
60 $\tilde{\nu}$=1292	3.444 52.06	2.26	878	0.0457	5.157 0.305	1.0162	1.426 $x10^{-2}$	0.492	858
61 $\tilde{\nu}$=1292	4.417 52.03	2.94	1425	0.0741	3.130 0.357	1.1047	1.342 $x10^{-2}$	0.463	1313
62 $\tilde{\nu}$=1294	5.366 52.03	2.85	1375	0.0715	3.107 0.386	1.6137	1.891 $x10^{-2}$	0.652	1787

4. C_2H_4 ($\tilde{\nu}$=900-1000, $\Delta\tilde{\nu}$=100)

Run No. $\tilde{\nu}$(cm^{-1})	y' ℓ(cm)	I_{pp}	C_i(ppm) $=p_i$(atm) $x10^6$	x_i	$k_{\tilde{\nu}}$ W_B	y= $\left(\frac{y'S_m}{2\pi I_{pp}}\right)$	$\mathscr{K}_{\tilde{\nu}}$	$\frac{\mathscr{K}_{\tilde{\nu}}}{\bar{\mathscr{K}}}$	$N_C=\left[\frac{6.667x10^4 y}{k_{\tilde{\nu}}\Delta\tilde{\nu}W_B(\mathscr{K}_{\tilde{\nu}}/\bar{\mathscr{K}})_a}\right]$
52 $\tilde{\nu}$=988	0.970 52.06	3.01	217	0.0113	11.45 0.340	0.2548	5.845 $x10^{-3}$	0.202	216
53 $\tilde{\nu}$=988	1.312 52.03	3.04	332	0.0173	9.015 0.340	0.3691	7.052 $x10^{-3}$	0.243	397
54 $\tilde{\nu}$=988	1.036 52.03	3.15	102	0.00531	17.51 0.340	0.2446	7.787 $x10^{-3}$	0.269	136
58 $\tilde{\nu}$=988	0.846 52.04	2.77	416	0.0216	8.009 0.337	0.2096	3.607 $x10^{-3}$	0.124	256
59 $\tilde{\nu}$=988	0.677 52.06	2.67	432	0.0225	7.754 0.354	0.1797	2.937 $x10^{-3}$	0.101	216
60 $\tilde{\nu}$=988	0.942 52.06	2.26	292	0.0152	9.970 0.311	0.2781	5.953 $x10^{-3}$	0.205	296
61 $\tilde{\nu}$=988	2.775 52.03	2.94	475	0.0247	7.380 0.354	0.694	1.081 $x10^{-2}$	0.373	877
62 $\tilde{\nu}$=988	0.609 52.03	2.85	458	0.0238	7.446 0.3681	0.183	2.818 $x10^{-3}$	0.0972	220